Radio-Science Performance Analysis Software

D. D. Morabito and S. W. Asmar
Telecommunications Systems Section

The Radio Science Systems Group (RSSG) provides various support functions for several flight project radio-science teams. Among these support functions are uplink and sequence planning, real-time operations monitoring and support, data validation, archiving and distribution functions, and data processing and analysis. This article describes the support functions that encompass radio-science data performance analysis. The primary tool used by the RSSG to fulfill this support function is the STBLTY program set. STBLTY is used to reconstruct observable frequencies and calculate model frequencies, frequency residuals, frequency stability in terms of Allan deviation, reconstructed phase, frequency and phase power spectral density, and frequency drift rates. In the case of one-way data, using an ultrastable oscillator (USO) as a frequency reference, the program set computes the spacecraft transmitted frequency and maintains a database containing the in-flight history of the USO measurements. The program set also produces graphical displays. Some examples and discussion on operating the program set on Galileo and Ulysses data will be presented.

I. Introduction

The radio science investigations of the different flight projects require a diverse set of tools for ensuring that acquired radio science data satisfy experimenter requirements. For example, the gravitational wave experiments on Galileo, Ulysses, Mars Observer, and Cassini each has specific stability requirements on the received signal frequency and amplitude. The Radio Science Systems Group (RSSG) utilizes various software tools to verify that the received data satisfy the requirements and that the required configurations are in place. STBLTY is the primary analysis tool used by the RSSG to characterize the performance of the radio science instrument. The STBLTY program set has been utilized by the RSSG to perform measurements of ultrastable oscillator (USO) frequency for the Galileo Solar Redshift Experiment [1,2], to characterize the performance of the Galileo Orbiter USO [3], to verify performance of the Mars Observer USO,[1] and to verify performance for the gravitational wave experiments on Galileo [2] and Ulysses [4]. The characterization of the Galileo USO is important for occultation radio science experiments that will be performed during the Jupiter tour [5]. This article will focus on describing the algorithms that are performed by the individual component programs of the STBLTY program set and will present examples using STBLTY on Galileo and Ulysses radio science data.

The version of STBLTY used for Voyager radio science was inherited by the Galileo and Ulysses radio science projects. This version was used primarily for one-way data occultation analysis, where

---

[1] D. D. Morabito, "Mars Observer 93-049 USO Test Processed Through STBLTY," JPL Interoffice Memorandum 3394-93-077 (internal document), Jet Propulsion Laboratory, Pasadena, California, June 17, 1993.

a baseline frequency signature was used to remove all effects other than those due to the planetary atmosphere. Hence, the inherited version did not have the stringent accuracy requirements needed for Galileo and Ulysses radio science experiments. In order to make STBLTY suitable for Galileo and Ulysses cruise data, several upgrades were made to the program set after the Voyager era (Neptune 1989). These upgrades included adding the capability of computing coherent two-way Doppler residuals, modeling the effects of a spinning spacecraft, upgrading the troposphere calibration model, introducing an ionosphere calibration algorithm using tracking system analytic calibration (TSAC) data as input, and estimating a more accurate trajectory model. The new trajectory model includes effects due to nutation, irregularities in Earth rotation (UT1–UTC), polar motion, equation of the equinoxes, zonal tides, and more comprehensive formulation of state vectors.

Figure 1 is a block diagram displaying the interconnections between the component programs of the STBLTY program set. Input radio science data consist of closed-loop data from the DSN tracking system in the form of archival tracking data files (ATDFs) or open-loop data from the radio science system in the form of original data record (ODR) tapes. The input celestial reference set (CRS) file from the Navigation Team of a supported project provides the spacecraft-state vectors necessary to model the spacecraft trajectory from the observable data.
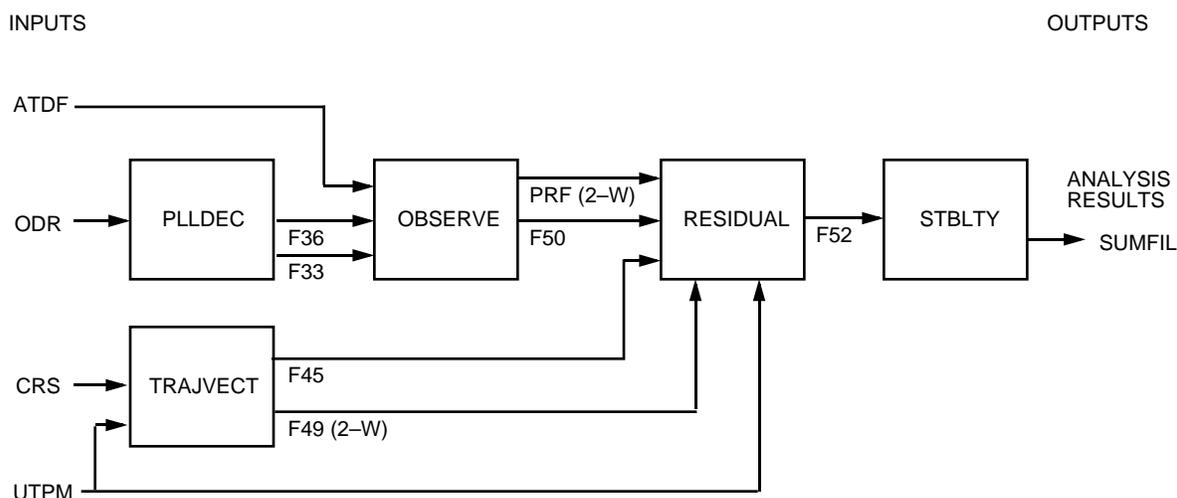

Fig. 1. The STBLTY program set block diagram displaying program names, input, output, and intermediate tape/file products.

The program TRAJVECT reads in body-centered spacecraft state vectors from the CRS file, translates the Earth-centered vectors to the location of the observing station, and performs light-time solutions. TRAJVECT produces a set of downlink state vectors at the time of signal reception (in file F45), and if data are two-way, produces a set of uplink vectors at the time of signal transmission (in file F49). These data sets are passed to the program RESIDUAL.

The closed-loop tracking system utilizes a phase-locked loop (PLL) that performs signal acquisition, lock-up, and detection in real time. The closed-loop data are conditioned by the Multi-Mission Navigation Team, which produces and delivers an ATDF to the RSSG. Among the quantities on an ATDF are Doppler counts, Doppler "pseudoresiduals" (residuals based on predicted frequencies used to tune the receivers), signal strengths (AGCs), and Doppler reference frequencies either in the form of a constant frequency or uplink ramps. OBSERVE reads the Doppler extractor cycle counts and Doppler extractor reference information from the ATDF and reconstructs these into received sky frequencies (in file F50). If data are two-way, OBSERVE writes the uplink ramps into the programmable ramp file (PRF).

The open-loop system mixes an incoming intermediate frequency (IF) signal with a signal whose frequency is a linear approximation of the predicted frequency, also known as the programmable oscillator control assembly (POCA) ramps. The baseband signal is passed through a filter whose bandpass is centered at the expected frequency and has a sufficiently wide bandwidth to allow for any unexpected signal frequency excursions. A set of analog-to-digital converters (ADCs) digitizes the received bandwidth and then writes the samples onto the ODR tapes. The program PLLDEC reads the ODR tapes and performs signal detection on the recorded samples, outputs an F36 file with the detected frequencies and signal strengths, and extracts the open-loop receiver tuning information (POCAs) from the ODR headers and writes these to an F33 file. The program OBSERVE reads the PLLDEC F36 and F33 output files and reconstructs the information into received sky frequencies and writes these in an F50 file that is passed to RESIDUAL.

The program RESIDUAL reads the observed sky frequency F50 file and, if the data are two-way, the PRF file output from OBSERVE and the spacecraft trajectory vectors from the TRAJVECT F45 (one-way or two-way) and F49 (two-way only) output files. RESIDUAL computes model frequencies from the F45 and F49 trajectory vectors and a spacecraft spin model. These model sky frequencies are subtracted from the observed sky frequencies to produce residual frequencies that are written onto the RESIDUAL output F52 file.

The F52 residual frequencies are input to the STBLTY program, which performs further corrections and produces Allan deviations, frequency and phase power spectral densities, and other quantities. In the case of one-way USO data, STBLTY computes the spacecraft transmitted frequency and writes out records for each pass onto a database summary file, SUMFIL, which is accessed by other programs for USO measurement analysis. The SUMFIL is also delivered to the radio science investigator, who performs an analysis for the purpose of measuring the solar gravitational redshift [1].

II. Program Descriptions

A more detailed description of each of the component programs of STBLTY follows.

A. PLLDEC—Open-Loop Data Signal Detection

The scheme employed for detecting signal frequency and power from the digitized samples of the open-loop system is a digital second-order phase-locked loop program called PLLDEC. The digitized samples output from the ADCs in the Deep Space Communications Complex (DSCC) spectrum processing (DSP) subsystem are written onto the ODR tapes (see Fig. 1) that are input to PLLDEC. A theoretical background that supplements the following discussion is given in [6], and a detailed description of a similar version of PLLDEC (using noncoherent AGC requiring high signal-to-noise ratio (SNR) signals) is contained in an internal memorandum.[2]

PLLDEC reads the set of digitized samples, $x(i), i = 1, \cdots, N$, from the ODR tape. An initial frequency, f_0, for the PLL is obtained from a fast Fourier transform (FFT) performed on an initial subset of samples. The output signal frequency, $y(nT)$, is expressed as a linear combination (recursive function) of the recorded samples, $x(i)$, and the previous output signal-frequency estimates, $y(iT)$.

The implemented phase-locked loop consists of a mixer (phase detector) and loop filter providing the forward gain path, $F(s) = (1 + as)/bs$; a low-pass filter, $K(s)$, for suppressing the mixer sum product (with negligible baseband response); and an integrator, $G(s) = 1/s$. The closed-loop transfer function (the transform of the PLL phase over the transform of the input phase) is given by

---

[2] A. Densmore, "A Digitally Implemented Phase-Locked Loop Detection Scheme for Analysis of Phase and Power Stability of a Calibration Tone," JPL Interoffice Memorandum Voyager RSST-88-016 (internal document), Jet Propulsion Laboratory, Pasadena, California, February 4, 1988.

$$L(s) = \frac{F(s)G(s)}{1 + F(s)G(s)} = \frac{1 + as}{1 + as + bs^2}$$

The desired s-domain transfer function of the second-order PLL of the output detected frequency to the input phase is given by

$$W(s) = \frac{s(1 + as)}{1 + as + bs^2}$$

The continuous time analysis of the discrete time PLL is justified by assuming that the product of the PLL noise bandwidth and sample period is much less than unity, $(B_{PLL}T << 1)$. In order to realize the digital PLL implementation, the bilinear transformation from s-space to z-transform space is employed:

$$s \simeq \frac{2}{T} \frac{1 - z^{-1}}{1 + z^{-1}} \tag{1}$$

It has been shown that this transformation outperforms others for the case of low sample rates [7].

By substituting Eq. (1) for s into $G(s)$, the following z-domain expression for the integrator is obtained:

$$G(z) = \frac{T}{2} \left(\frac{1 + z^{-1}}{1 - z^{-1}} \right) \tag{2}$$

By substituting Eq. (1) for s into $F(s)$, the corresponding z-domain function for the loop filter is obtained:

$$F(z) = \frac{T + 2a}{2b} \frac{\left[1 + z^{-1}((T - 2a)/(T + 2a)) \right]}{1 - z^{-1}} \tag{3}$$

The relations for a and b are given by

$$a = \frac{R + 1}{4B_{PLL}}$$

$$b = \frac{a^2}{R}$$

where R is the loop damping parameter, which is set equal to 2, the optimum value of loop performance specified by Jaffee and Rechtin [8] when the initial phase is unknown but uniformly distributed. A typical value for the one-sided loop bandwidth used for Galileo and Ulysses radio-science data processing is $B_{PLL} = 1$ Hz.

A single-pole low-pass filter is also employed to suppress the mixer sum product and has the following s-domain representation:

$$K(s) = \frac{1}{1 + (s/a)}$$

Using the bilinear transformation, the implemented z-domain transfer function of the low-pass filter is given by

$$K(z) = \frac{aT}{2+aT} \frac{1+z^{-1}}{[1-z^{-1}\left((2-aT)/(2+aT)\right)]} \tag{4}$$

where a is set equal to 10 B_{PLL}. The bilinear form of Eqs. (2), (3), and (4) are used to determine the appropriate coefficients that multiply the previous input samples and previous output values to yield each output estimate of signal phase or frequency.

The contribution to the Allan deviation due to additive white Gaussian noise (AWGN) over the PLL bandwidth B_{PLL} can be estimated from the following equation:

$$\sigma_y(\tau) = \frac{\sqrt{3B_{PLL}CNR^{-1}}}{2\pi f_0 \tau}$$

where B_{PLL} is the PLL bandwidth, Hz; CNR is the carrier signal-to-noise ratio of the signal; f_0 is the observing frequency, Hz; and τ is the time interval, s. By knowing the expected signal strengths and system noise temperatures, one can use this equation to estimate the B_{PLL} required to obtain an estimate of the AWGN contribution to the Allan deviation. By reducing B_{PLL} appropriately, one can reduce this contribution below other effects, thereby allowing visibility of those effects. Typical CNRs for Galileo and Ulysses result in AWGN contributions to the Allan deviations at 1000 s, which lie well below the measured values that are limited by media (for two-way Galileo and Ulysses) and USO (for Galileo one-way) when using 1 Hz for B_{PLL}.

B. TRAJVECT—Trajectory Vector Conditioning

The program TRAJVECT reads spacecraft state vectors from the CRS file, corrects Earth-center vectors to the observing-station location, and performs light-time solutions to yield a set of downlink state vectors at the time of signal reception, and (if two-way) performs a light-time solution to yield a set of uplink state vectors at the time of signal transmission. The conditioned set of state vectors is then passed to RESIDUAL. For discussions on how the NAV orbit determination solutions are performed, from which the CRS files are derived, the reader is referred to [9] for Galileo and [10] for Ulysses.

1. Input CRS File State Vectors. For cruise processing, where the gravitational effects of the planets are assumed negligible, it suffices that the CRS file contains EME 1950 (Earth mean equator and equinox of B1950.0) state vectors of the spacecraft relative to the Sun and the Earth, as follows:

$$\mathbf{x}^{\oplus-\mathbf{s}/\mathbf{c}}(t_k) = \text{Earth center-to-spacecraft position vector}$$
$$\mathbf{v}^{\oplus-\mathbf{s}/\mathbf{c}}(t_k) = \text{Earth center-to-spacecraft velocity vector}$$
$$\mathbf{x}^{\odot-\mathbf{s}/\mathbf{c}}(t_k) = \text{Sun-to-spacecraft position vector}$$
$$\mathbf{v}^{\odot-\mathbf{s}/\mathbf{c}}(t_k) = \text{Sun-to-spacecraft velocity vector}$$

where k is the index of the vectors which are evenly spaced in time, T s apart. The time tag, t_k, is referenced at the spacecraft in ephemeris time in seconds past 1950.0.

2. Conversion to Sun Center. The state vectors from the CRS file are referred to Sun center using the following translations:

$$\mathbf{x}^{\oplus-\odot}(t_k) = \mathbf{x}^{\oplus-\mathbf{s/c}}(t_k) - \mathbf{x}^{\odot-\mathbf{s/c}}(t_k) \tag{5}$$

$$\mathbf{x}^{\mathbf{s/c}-\odot}(t_k) = -\mathbf{x}^{\odot-\mathbf{s/c}}(t_k) \tag{6}$$

$$\mathbf{v}^{\oplus-\odot}(t_k) = \mathbf{v}^{\oplus-\mathbf{s/c}}(t_k)\left(\frac{+}{\text{rel}}\right) - \mathbf{v}^{\odot-\mathbf{s/c}}(t_k) \tag{7}$$

$$\mathbf{v}^{\mathbf{s/c}-\odot}(t_k) = -\mathbf{v}^{\odot-\mathbf{s/c}}(t_k) \tag{8}$$

where the $(+/\text{rel})$ notation means that the velocities add relativistically.

3. Calculation of Observing Station Vectors. TRAJVECT translates the Earth–Sun vectors [Eqs. (5) and (7)] to the location of the observing station. The station–Earth vectors are computed in the EME 1950 frame and are added to the Earth–Sun vectors [Eqs. (5) and (7)] to produce the required station-to-Sun state vectors. Among the corrections applied to the station vectors are precession, nutation, UT1–UTC, polar motion, equation of the equinoxes, and solid Earth tides.

A table of station locations in cylindrical coordinates (referenced to the mean pole, equator, and prime meridian of 1900.05) are read to obtain the observing station coordinates: radius off the spin axis, r_s (km); height above the equatorial plane, z (km); and longitude in degrees east of the Greenwich meridian, λ. Thus, the body-fixed station vector in rectangular coordinates is

$$\mathbf{x}^{\mathbf{dss}} = \begin{bmatrix} r_s & \cos & \lambda \\ r_s & \sin & \lambda \\ & z & \end{bmatrix}$$

Several notations are used to denote time: the corresponding Julian date of t_k,

$$t_k^{JD} = \frac{t_k}{86,400} + 2,433,282.5$$

the number of Julian centuries of 36,525 mean solar days that have elapsed since 1950.0, T_k,

$$T_k = \frac{t_k}{3,155,760,000}$$

and the difference of ephemeris time (ET) and universal time (UT1), Δt_k.

To translate the station vectors to the frame of the current epoch, several translations and rotations are applied. Polar motion matrix rotations are applied, and the vectors are then rotated to the correct position in the frame of the current epoch. The rotation matrices that perform these corrections use values of universal time and polar motion obtained from the monthly publications of the International Earth Rotation Service (IERS). These values are interpolated to the appropriate time tag, t_k, of the vectors, yielding the Earth orientation values of Δt_{UT1R} (UT1R–UTC) and polar motion X_p and Y_p. The Δt_{UT1R} is further corrected by adding the effects of short-period zonal tides (monthly and fortnightly), to yield Δt_{UT1}. The zonal tides are computed using the formulation of Yoder et al. [11].

The angle of the Greenwich meridian at the current epoch, corrected for variation in Earth rotation, $\alpha_G(t_k)$, is known as Greenwich mean sidereal time, or the Greenwich hour angle of the mean equinox of date, and is given by

$$\alpha_G(t_k) = \alpha_0(t_k) + \alpha_1(t_k) + \alpha_2(t_k) + \alpha_3(t_k) \tag{9}$$

where $\alpha_0(t_k) = -(1.002737909294 + T_k 0.589 \times 10^{-10})((\Delta t_k)/240) + 100.0755426042 + T_k^2 0.0003870833$ is the fraction of a turn (in degrees) of the Earth over T_k Julian centuries, $\alpha_1(t_k) = MOD[(t_k/240), 360]$ is the fraction of a turn (in degrees) due to daily rotation, $\alpha_2(t_k) = MOD[36,000T_k, 360]$ is the fraction of a turn (in degrees) due to the revolution of the Earth in its orbit, and $\alpha_3(t_k) = 0.7693120833T_k$ is the fraction of a turn (in degrees) over T_k Julian centuries, which accounts for the slowing down of the Earth due to the exertion of tidal forces.

The nutation model used by the program set is the International Astronomical Union (IAU) 1980, or Wahr nutation model, which was adopted by the IAU in 1984 and uses a series developed by Wahr based on the nutation model of P. K. Seidelmann [12]. The expected accuracy of this model (1 milliarc) [13], translates to about a 1-mHz error at 8.4 GHz, but is expected to be constant over a tracking pass. The angles of nutation estimated from this model are $\Delta\epsilon$, the nutation in obliquity; $\Delta\Psi$, the nutation in longitude; and ϵ_m, the mean obliquity of the ecliptic. The derivatives are computed from the differences of the nutation angles evaluated at two slightly different times divided by the time difference. The obliquity is added to the mean obliquity to yield the true obliquity of the ecliptic, ϵ.

The Greenwich mean sidereal time in Eq. (9), $\alpha_G(t)$, is converted to Greenwich apparent sidereal time, $\alpha_{GA}(t)$ (the Greenwich hour angle of the true equinox of date), by applying the correction of the equation of the equinoxes:

$$\alpha_{GA}(t_k) = \alpha_G(t_k) + \Delta\Psi\cos\epsilon$$

The space-fixed station vector projected in the celestial frame at t_k (the position of date) is computed from the body-fixed station vector by applying a series of rotations that corrects for polar motion ($\mathbf{R_1}$ and $\mathbf{R_2}$) and Earth rotation ($\mathbf{R_3}$). This "true of-date" space-fixed station vector is corrected for nutation ($\mathbf{N}$), which performs the rotation from the true of-date equator and equinox to the "mean of-date" equator and equinox. Finally, the station vector is rotated from the mean of-date equator to the mean equator of the reference epoch (EME 1950) using the precession rotation matrix, $\mathbf{P}$. See the Appendix for definitions of $\mathbf{P}$ and $\mathbf{N}$. The rotation matrices $\mathbf{R_1}, \mathbf{R_2}$, and $\mathbf{R_3}$ are given by

$$\mathbf{R_3}(\alpha_{GA}(t_k)) = \begin{bmatrix} \cos\alpha_{GA}(t_k) & -\sin\alpha_{GA}(t_k) & 0 \\ \sin\alpha_{GA}(t_k) & \cos\alpha_{GA}(t_k) & 0 \\ 0 & 0 & 1 \end{bmatrix}$$

$$\mathbf{R_2}(X_p) = \begin{bmatrix} \cos X_p & 0 & -\sin X_p \\ 0 & 1 & 0 \\ \sin X_p & 0 & \cos X_p \end{bmatrix}$$

$$\mathbf{R_1}(Y_p) = \begin{bmatrix} 1 & 0 & 0 \\ 0 & \cos Y_p & \sin Y_p \\ 0 & -\sin Y_p & \cos Y_p \end{bmatrix}$$

The station position vector in EME 1950 coordinates is computed as follows:

$$\mathbf{x^{dss-\oplus}}(t_k) = \mathbf{PN}[\mathbf{R_3R_2R_1 x^{dss}} + \Delta\vec{\mathbf{x}}_{tides}] \tag{10}$$

where $\mathbf{R_1}, \mathbf{R_2}$, and $\mathbf{R_3}$ are the "Earth platform" rotation matrices given above, $\mathbf{N}$ is the nutation rotation matrix, $\mathbf{P}$ is the precession rotation matrix, and $\Delta\mathbf{x}_{tides}(t_k)$ designates the perturbations due to solid Earth tides which, along with velocity perturbations, $\Delta\mathbf{v}_{tides}$, are induced by the Sun and Moon.[3]

The station velocity vector is given by[4,5,6]

$$\mathbf{v}^{\mathbf{dss}-\oplus}(t_k) = [\dot{\mathbf{P}}\mathbf{N} + \mathbf{P}\dot{\mathbf{N}}][\mathbf{R_3}\mathbf{R_2}\mathbf{R_1}\mathbf{x}^{\mathbf{dss}} + \Delta\mathbf{x}_{tides}(t_k)] + \mathbf{P}\mathbf{N}[\dot{\mathbf{R}}_{\mathbf{3}}\mathbf{R_2}\mathbf{R_1}\mathbf{x}^{\mathbf{dss}} + \Delta\mathbf{v}_{tides}(t_k)] \qquad (11)$$

where the $\dot{\mathbf{N}}$ and $\dot{\mathbf{P}}$ matrices (see the Appendix) denote the derivatives of the nutation and precession matrices, respectively, $\Delta\mathbf{v}_{tides}(t_k)$ is the station velocity perturbations due to tides, and $\dot{\mathbf{R}}_{\mathbf{3}}$ is given by

$$\dot{\mathbf{R}}_{\mathbf{3}}(\alpha_{GA}(t_k)) = \begin{bmatrix} -\sin\alpha_{GA}(t_k) & -\cos\alpha_{GA}(T_k) & 0 \\ \cos\alpha_{GA}(t_k) & -\sin\alpha_{GA}(t_k) & 0 \\ 0 & 0 & 0 \end{bmatrix}$$

4. Light-Time Solutions. The light-time solution is performed as follows. First, an initial estimate of the one-way light time is made using Eqs. (5) and (6):

$$\tau_0(t_k) = \frac{|\mathbf{x}^{\oplus-\odot}(t_k) - \mathbf{x}^{\mathbf{s/c}-\odot}(t_k)|}{c}$$

where the "0" subscript denotes the initial estimate. The ith estimate of the time tag of downlink reception a one-way light time later is made as follows:

$$t_{k,i} = t_k + \tau_i(t_{k,i-1}) \qquad (t_{k,0} = t_k) \qquad (12)$$

The three sets of vectors with time tags, t_{l-1}, t_l, and t_{l+1}, lying closest to the estimated received time, $t_{k,i}$, are quadratically interpolated to yield estimates of the state vectors at $t_{k,i}$. The station–Earth vectors [Eqs. (10) and (11)] are evaluated at $t_{k,i}$ and added to the Earth–Sun vectors (Eqs. (5) and (7) interpolated at $t_{k,i}$) as follows:

$$\mathbf{x}^{\mathbf{dss}-\odot}(t_{k,i}) = \mathbf{x}^{\mathbf{dss}-\oplus}(t_{k,i}) + \mathbf{x}^{\oplus-\odot}(t_{k,i}) \qquad (13)$$

$$\mathbf{v}^{\mathbf{dss}-\odot}(t_{k,i}) = \mathbf{v}^{\mathbf{dss}-\oplus}(t_{k,i}) \left(\frac{+}{\text{rel}}\right) \mathbf{v}^{\oplus-\odot}(t_{k,i}) \qquad (14)$$

The correction to the light-time of the next iteration is

---

[3] T. D. Moyer, "Correction to Earth Fixed Station Coordinates Due to Solid Earth Tides, Ocean Loading, and Pole Tides and Calculation of Periodic Terms of UT1," JPL Engineering Memorandum 314-505 (internal document), Jet Propulsion Laboratory, Pasadena, California, July 4, 1991.

[4] N. A. Mottinger and T. D. Moyer, "A Close Encounter With a Doppler Observable," JPL Interoffice Memorandum 314.5-1025 (internal document), Jet Propulsion Laboratory, Pasadena, California, June 18, 1984.

[5] T. D. Moyer, "Proposed Changes to ODP Transformation Between Body-Fixed and Space-Fixed Coordinates for the Planets and the Sun," JPL Engineering Memorandum 314-271 (internal document), Jet Propulsion Laboratory, Pasadena, California, June 16, 1982.

[6] T. D. Moyer, "Time Derivative and Partial Derivatives of the Body-Fixed to Space-Fixed Coordinate Transformation for the Sun, Planets and Planetary Satellites," JPL Engineering Memorandum 314-379 (internal document), Jet Propulsion Laboratory, Pasadena, California, August 22, 1985.

$$\Delta\tau_{i+1}(t_{k,i}) = \frac{|\mathbf{x^{dss-\odot}}(t_{k,i}) - \mathbf{x^{s/c-\odot}}(t_{k,i})|}{c} - \tau_i(t_{k,i-1}) \qquad (15)$$

and the new light-time is

$$\tau_{i+1}(t_{k,i}) = \tau_i(t_{k,i-1}) + \Delta\tau_{i+1}(t_{k,i})$$

The time tag for the next iteration is refined as [Eq. (12), substituting $i+1$ for i]

$$t_{k,i+1} = t_k + \tau_{i+1}(t_{k,i})$$

The correction [Eq. (15)] is compared against a preset tolerance that should be tight enough for accurate vector determination given the stability requirements of the experiment being processed and the time spacing of the input CRS vectors. The current value used for Galileo and Ulysses cruise data is 10^{-4} s, assuming vectors separated by 30 s. Once the criterion is met, the iterative solution is completed and returns the estimated vectors at $t_{k,(i+1)}$. If the criterion is not met, then additional iterations are performed until it is satisfied. In the case of the uplink vectors, the procedure is the same except that a minus sign replaces the plus sign in the appropriate equations.

The time tag of the final iteration of the light-time solution for the downlink output vectors is redefined for notational convenience as

$$t_k^* \overset{\Delta}{=} t_k + \tau_{i+1}(t_{k,i}) = t_{k,i+1}$$

The M state vectors from the CRS file are processed this way such that a set of M heliocentric station and spacecraft state vectors referenced at times $t_k^*, k = 1, \cdots, M$ is produced in the EME 1950 reference frame. These vectors are passed to RESIDUAL via the downlink vector file F45 and uplink vector file F49. For downlink,

$$\mathbf{x_{dn}^{dss-\odot}}(t_k^*) = \text{station position}$$
$$\mathbf{v_{dn}^{dss-\odot}}(t_k^*) = \text{station velocity}$$
$$\mathbf{x_{dn}^{s/c-\odot}}(t_k^*) = \text{spacecraft position}$$
$$\mathbf{v_{dn}^{s/c-\odot}}(t_k^*) = \text{spacecraft velocity}$$

For uplink,

$$\mathbf{x_{up}^{dss-\odot}}(t_l^*) = \text{station position}$$
$$\mathbf{v_{up}^{dss-\odot}}(t_l^*) = \text{station velocity}$$
$$\mathbf{x_{up}^{s/c-\odot}}(t_l^*) = \text{spacecraft position}$$
$$\mathbf{v_{up}^{s/c-\odot}}(t_l^*) = \text{spacecraft velocity}$$

where the subscript k is the index of the kth vector in the F45 downlink vector file, and the subscript l is the index of the lth vector in the F49 uplink vector file.

C. OBSERVE—Sky Frequency Reconstruction

1. Closed-Loop System. The program OBSERVE reads in "Doppler" cycle counts from the closed-loop system, $\phi(t_j)$, along with information needed to compute the Doppler extractor reference frequency, $f_{ref}(t_j)$. The cycle counts consist of an integer number of counts output from the Doppler counter, plus a fractional term output from the Doppler resolver. The Doppler reference frequency may either be a constant synthesizer frequency (SIM), normally used as the reference during one-way data acquisition, or be computed from uplink ramps used as the reference during two-way data acquisition. The ramps used to tune the uplink frequency consist of a series of programmable frequencies and ramps that drive a digitally controlled oscillator (DCO), which is multiplied up and input to the exciter that drives the transmitter. The ramps are written to the PRF file, which is input to RESIDUAL, where they are used to reconstruct the uplink frequencies for two-way data.

For closed-loop data read off an ATDF for a standard Deep Space Station (DSS), OBSERVE computes the received biased Doppler frequencies from the accumulated cycle counts as follows:

$$f_{dop}(t_j) = \frac{\phi(t_{j+1}) - \phi(t_{j-1})}{t_{j+1} - t_{j-1}}$$

In the case of a modulo reset, where $\phi(t_j)$ is less than $\phi(t_{j-1})$,

$$f_{dop}(t_j) = \frac{\phi(t_{j+1}) + 2^{32} - \phi(t_{j-1})}{t_{j+1} - t_{j-1}}$$

The Doppler frequency is converted to a 2.3-GHz sky frequency by

$$f^s(t_j) = 96\frac{240}{221}f_{ref}(t_j) \ -B \ (f_{dop}(t_j) - 10^6)$$

where 10^6 is the 1-MHz bias, B is the sign of the bias, f_{ref} is the Doppler extractor reference frequency interpolated to the time tag of the measured Doppler, and 240/221 is the spacecraft transponder ratio. For 8.4 GHz,

$$f^x(t_j) = 96\frac{880}{221}f_{ref}(t_j) \ -B \ (f_{dop}(t_j) - 10^6)$$

In the case of the 34-m high-efficiency (HEF) station, the 8.4-GHz frequency is given by[7]

$$f_{sky}(t_j) = \frac{880}{749}[32(4.68125f_{ref}(t_j) - 81.4125 \ 10^6) + 6500 \ 10^6] \ -B \ (f_{dop}(t_j) - 10^6)$$

2. Open-Loop System. For the case of open-loop data, the frequencies detected from the recorded samples by PLLDEC, f_{rec}, in the F36 file are converted to sky frequencies, f^s or f^x, using the tuning frequencies, f_{poca}, interpolated from the POCA offsets and ramps in the F33 file at the f_{rec} time tag. For the radio science IF–VF converter assembly (RIV) receivers,

---

[7] T. D. Moyer, "Change to the ODP and ODE for Processing X-Band Uplink Data," JPL Engineering Memorandum 314-430 (internal document), Jet Propulsion Laboratory, Pasadena, California, October 15, 1987.

$$f^s(t_j) = 3\left(f_{poca}(t_j) + \left(\frac{790}{11} \times 10^6\right)\right) + (1950 \times 10^6) - f_{samp} + f_{rec}(t_j)$$

$$f^x(t_j) = 11(f_{poca}(t_j) - \left(10 \times 10^6\right) + \left(8050 \times 10^6\right) - 3f_{samp} + f_{rec}(t_j)$$

where f_{samp} is the sampling frequency of the recorded samples. For the multimission receivers (MMRs),

$$f^s(t_j) = 48f_{poca}(t_j) + \left(300 \times 10^6\right) - \frac{3}{4}f_{samp} + f_{rec}(t_j)$$

$$f^x(t_j) = \frac{11}{3}\left[48f_{poca}(t_j) + \left(300 \times 10^6\right) - \frac{3}{4}f_{samp}\right] + f_{rec}(t_j)$$

The observed sky frequencies from OBSERVE are input to RESIDUAL, where model and residual frequencies are calculated.

D. RESIDUAL—Residual Frequency Calculation

The program RESIDUAL reads the sky frequencies from the OBSERVE output F50 file and the state vectors from the TRAJVECT output F45 and F49 files to compute model frequencies based on the spacecraft trajectory, and produces frequency residuals for either 2.3 GHz, 8.4 GHz, or differenced S-3/11X data. RESIDUAL applies a polarization-dependent correction for a spinning spacecraft[8] and can estimate and remove a sinusoidal signature induced by an off-axis antenna on a spinning spacecraft (e.g., low-gain antenna (LGA)-2 on Galileo).

1. Spin Correction. For the constant spin correction, specific default values are built into the code to account for different spacecraft configurations. This correction assumes the 2.3-GHz one-way default values for f_{spin} shown in Table 1 (note that Galileo has a 3-rpm spin rate and Ulysses has a 5-rpm spin rate). This correction could also be obtained from attitude-control telemetry data and the defaults therefore overridden. For Galileo passes involving LGA-2, the spin rate could also be solved for from a three-parameter sinusoid fit of the trajectory corrected residuals.

Table 1. One-way default values for f_{spin}.

Spacecraft	Antenna	Spin mode	$f_{spin}^{S,1\text{-}way}$, Hz
Galileo	LGA1, HGA	Dual	0.052
	LGA2	Dual	−0.052
	LGA1, HGA	All	0.048
	LGA2	All	−0.048
Ulysses			−0.0833
Any other			0.00

RESIDUAL applies the appropriate spin correction to the sky frequency depending upon the spacecraft spin configuration and frequency band. If the data are 2.3-GHz one-way, f_{spin} is applied as given in Table 1. For the case of two-way data with a 2.3-GHz downlink and a 2.3-GHz uplink,

[8] P. Priest and J. Breidenthal, "Galileo Spin Effects," JPL Interoffice Memorandum 3393-90-186 (internal document), Jet Propulsion Laboratory, Pasadena, California, November 30, 1990.

$$f_{spin}^{S/S} = \left(\frac{240}{221} + 1\right) f_{spin}^{S,1-way}$$

For the case of two-way data with an 8.4-GHz downlink and a 2.3-GHz uplink,

$$f_{spin}^{S/X} = \left[\frac{240}{221}\frac{11}{3} + 1\right] f_{spin}^{S,1-way}$$

For the case of dual-frequency S–X residuals, the spin correction applied is given by

$$f_{spin}^{S-X} = \frac{8}{11} f_{spin}^{S,1-way}$$

2. One-Way Data Processing. The state vectors from the TRAJVECT F45 file are interpolated to the time tag of the observable frequency (t_i^{dss} at the observing station and $t_i^{s/c}$ at the spacecraft) and are used to estimate the downlink Doppler correction factors:

$$d_1 = \sqrt{\frac{(c - |\mathbf{v}^{s/c-\odot}(t_i^{s/c})|)(c + |\mathbf{v}^{s/c-\odot}(t_i^{s/c})|)}{c^2}} \tag{16}$$

$$d_2 = 1 - \frac{\mathbf{v}^{dss-\odot}(t_i^{dss})}{c} \cdot \frac{\mathbf{x}^{dss-\odot}(t_i^{dss}) - \mathbf{x}^{s/c-\odot}(t_i^{s/c})}{|\mathbf{x}^{dss-\odot}(t_i^{dss}) - \mathbf{x}^{s/c-\odot}(t_i^{s/c})|} \tag{17}$$

$$d_3 = 1 - \frac{\mathbf{v}^{s/c-\odot}(t_i^{s/c})}{c} \cdot \frac{\mathbf{x}^{dss-\odot}(t_i^{dss}) - \mathbf{x}^{s/c-\odot}(t_i^{s/c})}{|\mathbf{x}^{dss-\odot}(t_i^{dss}) - \mathbf{x}^{s/c-\odot}(t_i^{s/c})|} \tag{18}$$

$$d_4 = \sqrt{\frac{[c - |\mathbf{v}^{dss-\odot}(t_i^{dss})|][c + |\mathbf{v}^{dss-\odot}(t_i^{dss})|]}{c^2}} \tag{19}$$

The gravitational redshift correction factors that account for the frequency shifts due to the masses of the Sun and the Earth, evaluated at t_i, are given by

$$d_\odot = \frac{G\,M_\odot}{c^2}\left[\frac{1}{|\mathbf{x}^{dss-\odot}|} - \frac{1}{|\mathbf{x}^{s/c-\odot}|}\right]$$

$$d_\oplus = \frac{G\,M_\oplus}{c^2}\left[\frac{1}{|\mathbf{x}^{dss-\oplus}|} - \frac{1}{|\mathbf{x}^{s/c-\oplus}|}\right]$$

The radiated 2.3-GHz frequency of the spacecraft is computed from the received frequency of the first data point as follows:

$$f_{s/c}(t_1) = \frac{f^s(t_1)}{(d_1 d_2 / d_3 d_4) + d_\odot + d_\oplus} + f_{spin}$$

where the Doppler and redshift terms are evaluated at t_1. The estimated sky frequencies (evaluated at t_i) are computed from this transmitted spacecraft frequency at the first data point (evaluated at t_1) using the above correction factors (evaluated at t_i) as follows:

$$\hat{f}^s(t_i) = f_{s/c}(t_1) \left[\frac{d_1 d_2}{d_3 d_4} + d_\odot + d_\oplus \right]$$

For the one-way case, the residuals are defined such that the first data point is anchored to zero. Given the set of observable frequencies output from the OBSERVE F50 file, $f^s(t_i)$, the estimated frequency for the first data point is, by definition,

$$\hat{f}^s(t_1) = f^s(t_1)$$

The residual frequencies are computed by differencing the model from the observable as follows:

$$\Delta f^s(t_i) = f^s(t_i) - \hat{f}^s(t_i)$$

The residual frequencies and the spacecraft transmitted frequency are passed to STBLTY in the F52 file for further processing.

3. Two-Way Data Processing. This section discusses the computations of two-way Doppler frequencies and residuals. The downlink Doppler corrections [Eqs. (16)–(19)] are evaluated at the time tag of the received signal frequency, t_i^{dss}, as described in the previous section. In addition, the uplink vectors from the F49 file are interpolated to the time of uplink signal transmission, t_i^{up}, and the Doppler correction terms for the uplink signal leg are similarly computed as follows:

$$u_1(t_i) = \sqrt{\frac{(c - |\mathbf{v^{dss-\odot}}(t_i^{up})|)(c + |\mathbf{v^{dss-\odot}}(t_i^{up})|)}{c^2}} \tag{20}$$

$$u_2(t_i) = 1 - \frac{\mathbf{v^{s/c-\odot}}(t_i^{s/c})}{c} \cdot \frac{\mathbf{x^{s/c-\odot}}(t_i^{s/c}) - \mathbf{x^{dss-\odot}}(t_i^{up})}{|\mathbf{x^{s/c-\odot}}(t_i^{s/c}) - \mathbf{x^{dss-\odot}}(t_i^{up})|} \tag{21}$$

$$u_3(t_i) = 1 - \frac{\mathbf{v^{dss-\odot}}(t_i^{up})}{c} \cdot \frac{\mathbf{x^{s/c-\odot}}(t_i^{s/c}) - \mathbf{x^{dss-\odot}}(t_i^{up})}{|\mathbf{x^{s/c-\odot}}(t_i^{s/c}) - \mathbf{x^{dss-\odot}}(t_i^{up})|} \tag{22}$$

$$u_4(t_i) = \sqrt{\frac{(c - |\mathbf{v^{s/c-\odot}}(t_i^{s/c})|)(c + |\mathbf{v^{s/c-\odot}}(t_i^{s/c})|)}{c^2}} \tag{23}$$

The radiated frequency at the time of signal transmission, t_i^{up}, is obtained from the uplink ramps in the PRF file, interpolated at t_i^{up}, and then multiplied up to sky frequency, $f_u^{st}(t_i^{up})$. The estimated 2.3-GHz received frequency is computed as follows:

$$\hat{f}^s(t_i) = \left[f_u^{st}(t_i^{up}) \frac{240}{221} \frac{u_1 u_2}{u_3 u_4} - f_{spin}^{s/s} \right] \frac{d_1 d_2}{d_3 d_4}$$

The 2.3-GHz residual frequency is computed from the observed and estimated received frequencies at time t_i as follows:

$$\Delta f^s(t_i) = f^s(t_i) - \hat{f}^s(t_i)$$

Likewise, for 8.4 GHz,

$$\hat{f}^x(t_i) = \left[f_u^{st}\left(t_i^{up}\right) \frac{11}{3} \frac{240}{221} \frac{u_1 u_2}{u_3 u_4} - f_{spin}^{s/x} \right] \frac{d_1 d_2}{d_3 d_4}$$

$$\Delta f^x(t_i) = f^x(t_i) - \hat{f}^x(t_i)$$

4. Correction for Off-Axis Antenna on a Spinning Spacecraft. A sinusoidal signature due to an off-axis antenna on a spinning spacecraft can be removed by fitting a three-parameter model to the bias-corrected residuals:

$$\Delta \overline{f}^s(t_i) = C_1 \sin(C_2 t_i + C_3)$$

where t_i is the time tag of the data point. The spacecraft transmitted frequency is corrected so that it is referenced to the phase center of the spacecraft spin. This is done by removing the value at the first data point:

$$f_{s/c}(t_1) = f_{s/c}(t_1) - C_1 \sin(C_3)$$

The residuals are adjusted accordingly:

$$\Delta f_c^s(t_i) = \Delta f^s(t_i) + C_1 \sin(C_2 t_i + C_3) - C_1 \sin(C_2 t_1 + C_3)$$

The spacecraft transmitted frequency, $f_{s/c}$, is passed to the program STBLTY in the F52 file along with other header information, observed frequencies, and residuals.

E. STBLTY—Media Correction, Display Plots, and Output File

STBLTY is the final program that applies additional corrections to the data, writes out records to a database file for USO and gravitational redshift analysis, and produces plots. At this point, the residual frequencies $\Delta f^s(t_i)$ and/or $\Delta f^x(t_i)$ for L data points $i = 1, 2, \cdots, L$ are read in from the RESIDUAL F52 output file. If both bands are available, STBLTY then combines the observable frequencies to produce the differential data type:

$$\Delta f^{sx}(t_i) = f^s(t_i) - \frac{3}{11} f^x(t_i) \tag{24}$$

For one-way data, the spacecraft transmitted frequency referenced to the first data point, $f_{s/c}(t_1)$, is passed in the header.

1. Ionosphere/Charged-Particle Calibration. The charged particle effect can be "removed" from the radio science data in one of two ways: (1) When dual-frequency data are available, a differential

correction computed from the differential data type, Eq. (24), is applied to the individual frequency bands or (2) a TSAC-supplied polynomial describing the ionosphere path delay signature can be converted into frequency and removed from the frequency residuals. The TSAC correction removes ionospheric effects for either dual- or single-band downlink passes.

For the case where two simultaneous downlink frequency channels exist, the charged particle can be removed using the differential frequency type $f^s - 3f^x/11$, given in Eq. (24). Given that the frequency residuals to be corrected are $\Delta f^s(t_i)$ for 2.3 GHz and $\Delta f^x(t_i)$ for 8.4 GHz, the corrected residuals are

$$\Delta f_c^s(t_i) = \Delta f^s(t_i) - \frac{121}{112}\Delta f^{sx}(t_i)$$

for a one-way 2.3-GHz downlink;

$$\Delta f_c^x(t_i) = \Delta f^x(t_i) - \frac{33}{112}\Delta f^{sx}(t_i)$$

for a one-way 8.4-GHz downlink;

$$\Delta f_c^s(t_i) = \Delta f^s(t_i) - \left[\frac{240}{221}\frac{121}{112} + \frac{121}{112}\right]\Delta f^{sx}(t_i)$$

for a two-way 2.3-GHz uplink/2.3-GHz downlink; and

$$\Delta f_c^x(t_i) = \Delta f^x(t_i) - \left[\frac{240}{221}\frac{121}{112} + \frac{33}{112}\right]\Delta f^{sx}(t_i)$$

for a two-way 2.3-GHz uplink/8.4-GHz downlink, where the subscript c denotes the corrected value of the residual frequency.

The TSAC group produces and delivers ionosphere calibration files to the RSSG, where they are archived and sometimes delivered to the radio science experimenters. The files contain polynomial coefficients describing the mapped ionosphere path delay in meters (referenced to a 2295-MHz carrier) for each DSCC and for each time period that overlaps a tracking pass for a given spacecraft. TSAC determines these coefficients from observations of Earth-orbiting satellites at each complex and maps to the line of sight of the spacecraft.

The TSAC coefficients and time tags are converted to frequency corrections in Hz (referenced to 2.3 GHz) by STBLTY. Given the start time, (t_b), and end time, (t_f), of the interval for which the polynomial is defined, and the polynomial coefficients $(a_i, i = 0, \cdots, 5)$, the ionosphere path delays to the spacecraft at regularly spaced intervals of time t_j are computed as follows:

$$\Delta\rho_{ion}(t_j) = \sum_{i=0}^{5} a_i x_j^i$$

where

$$x_j = 2\left[\frac{t_j - t_b}{t_f - t_b}\right] - 1$$

The path delays computed at time offsets $\pm T/2$ about t_j are differenced and scaled to yield the one-way 2.3-GHz ionosphere frequency correction at t_j:

$$f_{ion}^s(t_j) = \frac{f^s \left[\Delta\rho_{ion}\left(t_j + (T/2)\right) - \Delta\rho_{ion}\left(t_j - (T/2)\right) \right]}{cT}$$

Figure 2 is an example of a typical path delay profile derived from a TSAC polynomial. Figure 3 is the corresponding ionosphere frequency profile at 2.3 GHz.

The set of time tags, t_j, and corrections, $f_{ion}(t_j)$, that overlaps the tracking pass is used to perform the calibration only if dual-frequency charged-particle calibration was not previously performed. Given the frequency residual, $\Delta f^s(t_i)$ or $\Delta f^x(t_i)$, and the above ionosphere correction interpolated to time t_i, $f_{ion}^s(t_i)$, the corrected residuals are then computed as follows: For a one-way 2.3-GHz downlink,

$$\Delta f_c^s(t_i) = \Delta f^s(t_i) - f_{ion}^s(t_i)$$

for a one-way 8.4-GHz downlink,

$$\Delta f_c^x(t_i) = \Delta f^x(t_i) - \frac{3}{11} f_{ion}^s(t_i)$$

for a two-way 2.3-GHz uplink/2.3-GHz downlink,

$$\Delta f_c^s(t_i) = \Delta f^s(t_i) - f_{ion}^s(t_i) - \frac{240}{221} f_{ion}^s(t_i - t_r)$$

and for a two-way 2.3-GHz uplink/8.4-GHz downlink,

$$\Delta f_c^x(t_i) = \Delta f^x(t_i) - \frac{3}{11} f_{ion}^s(t_i) - \frac{11}{3} \frac{240}{221} f_{ion}^s(t_i - t_r)$$

where t_r is the round-trip light time.

For the case of differential $f^s - 3f^x/11$ two-way data, the contribution of the common 2.3-GHz uplink will be zero after differencing the two downlink channels. The remaining charged-particle contribution in the Δf^{sx} data type (SX) will be due to the downlink only. Therefore, this data type is corrected as follows:

$$\Delta f_c^{sx}(t_i) = \Delta f^{sx}(t_i) - \frac{8}{11} f_{ion}^s(t_i) \tag{25}$$

2. Troposphere Calibration. The troposphere calibration is performed after the ionosphere calibration so that the remaining time-dependent signature of the residuals over elevation angle more closely follows the troposphere ray-path function. The troposphere can be removed using either a model with a specified zenith troposphere path delay (default 2.1-m) or the zenith path delay can be fit and removed from the data if there is sufficient arc over elevation angle. The ray-path mapping function used is the CfA (Center for Astrophysics) mapping function [14]:
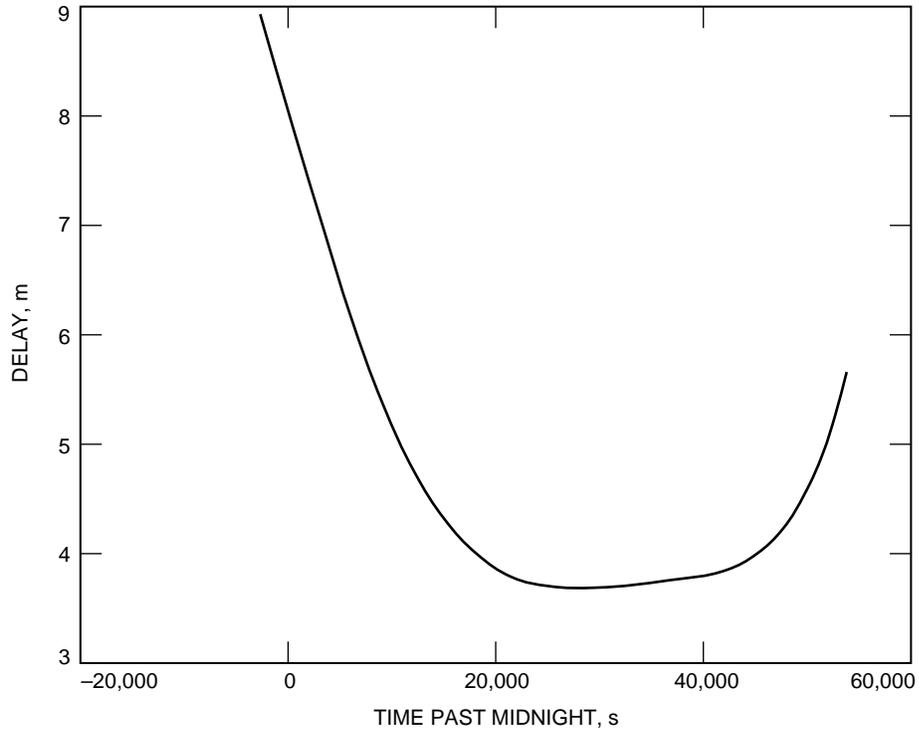
Fig. 2. An example of a typical ionosphere path delay profile derived from a TSAC polynomial.
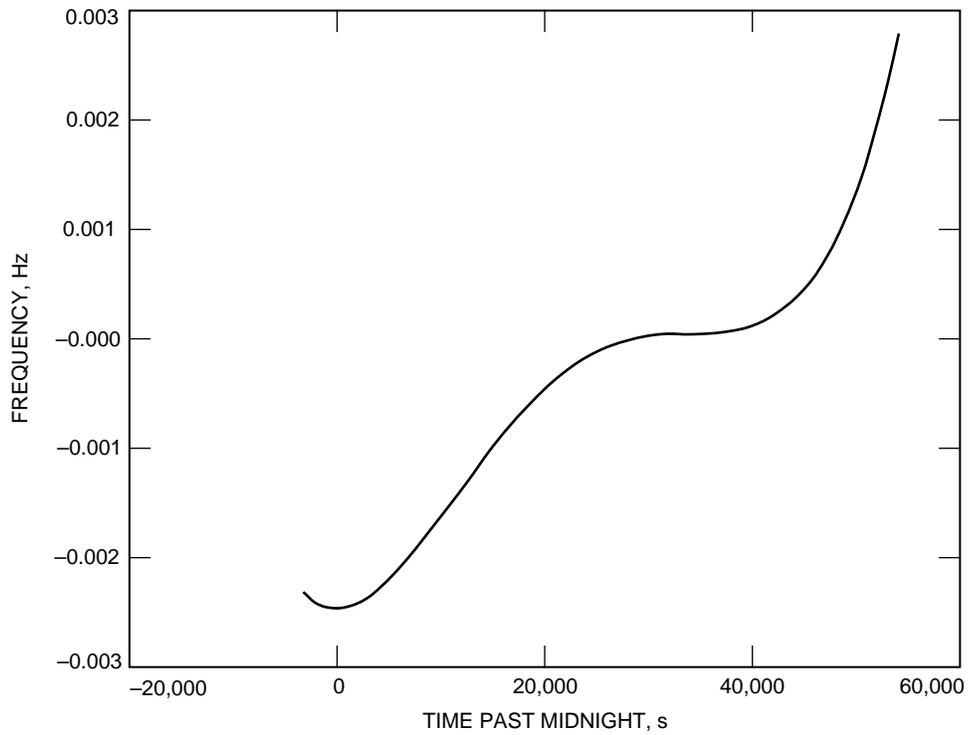

Fig. 3. An example of a typical frequency profile over a pass derived from the TSAC delay profile of Fig. 2.

$$R(t_i) = \frac{1}{\sin e(t_i) + (b_1/(\tan e(_i) + (b_2/(\sin e(t_i) + b_3))))}$$

where $e(t_i)$ is the elevation angle and the coefficients b_k are functions of meteorological parameters, given by

$$b_1 = 0.0002723[1 + (2.642 \times 10^{-4} p_0) - (6.400 \times 10^{-4} e_0) + (1.337 \times 10^{-2} T_o) - (8.550 \times 10^{-2} \alpha) \\ - (2.456 \times 10^{-2} h_2)]$$

$$b_2 = 0.0004703[1 + (2.832 \times 10^{-5} p_0) + (6.799 \times 10^{-4} e_0) + (7.563 \times 10^{-3} T_0) - (7.390 \times 10^{-2} \alpha) \\ - (2.961 \times 10^{-2} h_2)]$$

$$b_3 = -0.0090$$

Reasonable values of surface pressure ($p_0 = 900$ mbar), partial water vapor pressure ($e_0 = 5$ mbar), surface temperature ($T_0 = 292$ K), tropopause altitude ($h_2 = 12.2$ km), and dry model parameter ($\alpha = 5.0$) are used in the computation of these coefficients. This model is in agreement with predictions made by Lanyi [15] to the 1-cm level down to a 5-deg elevation angle.

The one-way troposphere correction to the observed 2.3-GHz frequency residual is given by

$$f_{trop}^s(t_i) = -\frac{f^s(t_i)\Delta\rho_z}{cT}\left[R\left(t_i + \frac{T}{2}\right) - R\left(t_i - \frac{T}{2}\right)\right]$$

where $f^s(t_i)$ is the downlink sky frequency, $\Delta\rho_z$ is the zenith troposphere path delay, c is the velocity of light, and $T/2$ is a chosen time offset about t_i. For the cases of two-way 2.3-GHz uplink/2.3-GHz downlink and 2.3-GHz uplink/8.4-GHz downlink, the corrections are

$$f_{trop}^s(t_i) = \frac{-f^s(t_i)\Delta\rho_z}{cT}\left(\left[R\left(t_i + \frac{T}{2}\right) - R\left(t_i - \frac{T}{2}\right)\right] + \frac{240}{221}\left[R\left(t_i + \frac{T}{2} - t_r\right) - R\left(t_i - \frac{T}{2} - t_r\right)\right]\right)$$

$$f_{trop}^x(t_i) = \frac{-f^x(t_i)\Delta\rho_z}{cT}\left(\left[R\left(t_i + \frac{T}{2}\right) - R\left(t_i - \frac{T}{2}\right)\right] + \frac{240}{221}\left[R\left(t_i + \frac{T}{2} - t_r\right) - R\left(t_i - \frac{T}{2} - t_r\right)\right]\right)$$

where t_r is the round-trip light time. The one-way frequency residuals are adjusted accordingly:

$$\Delta f_c^s(t_i) = \Delta f^s(t_i) - f_{trop}^s(t_i) + f_{trop}^s(t_1)$$

$$\Delta f_c^x(t_i) = \Delta f^x(t_i) - f_{trop}^x(t_i) + f_{trop}^x(t_1)$$

effectively removing the signature of the troposphere relative to the first data point, because $f_{s/c}(t_1)$ was evaluated here. A bias correction evaluated from the average of the corrected residuals is applied to the transmitted spacecraft frequency to refer it to the center of mass of the residuals. The spacecraft transmitted frequency at 2.3 GHz is corrected as follows:

$$f_{c,s/c}^s(t_{mid}) = f_{s/c}^s(t_1) + f_{trop}^s(t_1) + \overline{\Delta f_c^s}$$

where the last term is the average of the corrected residuals over the data span and t_{mid} is the time tag of the midpoint of the data acquisition interval.

The two-way frequency residuals are corrected for troposphere as follows:

$$\Delta f_c^s(t_i) = \Delta f^s(t_i) - f_{trop}^s(t_i)$$

$$\Delta f_c^x(t_i) = \Delta f^x(t_i) - f_{trop}^x(t_i)$$

III. STBLTY Performance Analysis Results and Discussion

The following sections will discuss examples using STBLTY on Galileo and Ulysses flight data.

A. Galileo Results

Examples of running STBLTY on Galileo radio science data will be presented in the following two sections.

1. One-Way Data. The results of routine processing of Galileo USO data using STBLTY will be briefly discussed in this section. For further details on this analysis of closed-loop one-way USO data acquired during the first 2 years of cruise (1989–1991), the reader is referred to [3].

Due to the undeployed high-gain antenna (HGA), only 2.3-GHz data from the LGA antennas were available. The passes were conducted weekly on the average, were typically 2 hours in duration, and were centered about meridian crossing where the troposphere effect was minimal. For troposphere calibration, it was sufficient to remove a model (versus fit and remove) using a default zenith path delay. The error incurred by not performing an ionosphere calibration is expected to be at the mHz level or below for a 2-hour pass centered about meridian crossing at 2.3 GHz.

The Allan deviation results were consistent with the values expected at the appropriate time intervals, given the known signal levels and noise mechanisms. At the short time intervals, the noise in the signal was dominated by thermal noise due to the low signal levels that were due to transmitting through the LGA. At the long time intervals, the noise in the signal was dominated by the USO itself. The transmitted USO-referenced spacecraft frequency followed a behavior that was consistent with known aging mechanisms of the USO, having an rms scatter of 17 mHz about a fitted aging model.

2. Two-Way Data. The testing of different calibration schemes using STBLTY on Galileo two-way 2.3-GHz data will be discussed in this section. STBLTY was run on three passes: (1) a DSS-63 tracking pass on day 91-123, (2) a DSS-63 pass on day 93-081, and (3) a DSS-14 pass on day 93-082. The latter two passes are from the 1993 Gravitational Wave Experiment.

Table 2 displays the processing results for these three passes using different calibration schemes. The first column denotes the year and day number of the pass; the next column is the DSN station identification; the next column denotes the ionosphere calibration employed (see the key for an explanation of the codes); the next column denotes the troposphere calibration employed (see the key for an explanation of the codes); the next column is the zenith path delay and uncertainty in the troposphere calibration (if the code in the TRP column is "F," this value is from the least-square fit); the next column is the slope from a linear fit of the residuals after calibrations have been performed; and the last four columns are the Allan deviations of the postcalibration residuals at 1, 10, 100, and 1000 s.

Four different calibration schemes were employed for each pass. The first run (ION:T, TRP:F) involved calibrating the ionosphere utilizing TSAC polynomial coefficients and calibrating the troposphere by fitting the model over the elevation angle for a zenith path delay and bias. The second run (ION:N,

TRP:F) involved no ionosphere calibration and calibrating the troposphere as described in the first scheme. The third run (ION:T, TRP:M) involved calibrating the ionosphere using TSAC polynomial coefficients and calibrating the troposphere by removing the model using the default zenith path delay of 2.1 m (no fitting performed). The last run (ION:N, TRP:N) did not employ any media calibration.

The zenith path delay for the TSAC ionosphere/troposphere fit run (T,F) for passes 91-123 and 93-081 are in reasonable agreement with the expected 2.1-m zenith path delay. The zenith path delay fit from the data when no ionosphere is removed (N,F) is consistently lower than those of the TSAC calibrated runs (T,F) and (T,M). This suggests that the TSAC calibration does contribute to removing nontropospheric trends from the data.

The linear slope of the residuals tends to increase in magnitude as fewer calibrations are performed. The magnitude of the linear slope tends to be smaller for the runs involving both troposphere fit and TSAC ionosphere calibration (T,F) and larger for the run involving no calibrations (N,N).

The Allan deviations at the time intervals of 1, 10 and 100 s do not differ significantly between the different schemes over each given pass. The Allan deviation at 1000 s for the three runs involving a troposphere calibration (T,F), (N,F), and (T,M) are in reasonable agreement. The 1000-s Allan deviations are consistent with values predicted due to solar plasma at the known solar elongation angles using the model of Armstrong, Woo, and Estabrook [16]. However, the Allan deviations at 1000 s are significantly larger for the no-media calibration case (N,N), clearly showing that the removal of the systematic troposphere signature with elevation angle is important for obtaining meaningful results at this time interval.

For Galileo at 2.3 GHz, trajectory errors of 0.018-mm/s in velocity translate to Allan deviations at 1000 s of about 6×10^{-14}. This lies below the 10^{-13} level expected due to plasma (for two-way data) and the instability of the USO (for one-way data).

Table 2. Galileo media calibration test results.

Pass, yr-day	DSS	ION	TRP	Zenith path delay, m	Linear slope, 10^{-7} Hz/s	$\sigma_y(1)$, 10^{-14}	$\sigma_y(10)$, 10^{-14}	$\sigma_y(100)$, 10^{-14}	$\sigma_y(1000)$, 10^{-14}
91-123	63	T	F	1.96 ± 0.03	0.12 ± 0.29	—	357	27.7	24.8
91-123	63	N	F	0.98 ± 0.03	0.16 ± 0.29	—	357	27.6	27.0
91-123	63	T	M	2.1	0.84 ± 0.29	—	357	27.7	25.0
91-123	63	N	N	—	-5.01 ± 0.29	—	357	27.7	38.2
93-081	63	T	F	2.17 ± 0.03	0.77 ± 0.27	1947	206	25.4	17.9
93-081	63	N	F	1.70 ± 0.04	1.55 ± 0.27	1947	206	25.5	23.3
93-081	63	T	M	2.1	0.58 ± 0.27	1947	206	25.4	18.4
93-081	63	N	N	—	-3.55 ± 0.27	1947	206	26.1	50.5
93-082	14	T	F	1.11 ± 0.04	0.39 ± 0.32	1808	194	26.9	14.5
93-082	14	N	F	0.80 ± 0.05	0.75 ± 0.31	1808	195	26.9	17.9
93-082	14	T	M	2.1	2.73 ± 0.32	1808	195	26.9	13.4
93-082	14	N	N	—	-1.14 ± 0.32	1808	195	27.1	29.1

T = TSAC ionosphere calibration.
D = Dual-frequency ($f^s - 3f^x/11$) charged-particle calibration.
N = No calibration performed.
F = Troposphere calibration (model removed using fit zenith path delay).
M = Troposphere calibration (model removed using default zenith path delay).

B. Ulysses Results

For Ulysses, two sets of two-way data were analyzed: (1) closed-loop data from a dual-band pass from the first opposition 91-004 (DSS 14) and (2) open-loop data from a dual-band pass from the second opposition 92-064 (DSS 14). Table 3 displays the results for these data sets and for each of the applicable data types within each pass. For the single-band data (2.3 and 8.4 GHz), the following runs were performed: (1) TSAC ionosphere and troposphere fit (T,F), (2) dual-frequency calibration of charged particles, and troposphere fit (D,F), (3) no ionosphere/charged-particle and troposphere fit (N,F), and (4) TSAC ionosphere and troposphere model removed using the default zenith path delay (T,M). The no-calibration case (N,N) is not presented in this table since the (N,N) Galileo runs (Section III.A) clearly illustrate the degradation when not applying a media correction. The description of Table 3 is the same as that of Table 2 in the proceeding section except that the data type code (S, X, or SX) follows the year-day number in the first column.

Figure 4 is a plot of the 8.4-GHz residuals for pass 91-004 for the fully calibrated (T,F) run. Figure 5 is a plot of the averaged residuals where every 60 points have been averaged to allow long period trends to be easily examined. Figure 6 is a plot of the reconstructed phase for this pass, and Fig. 7 is a plot of the corresponding Allan deviation. Figure 8 is a plot of the averaged residuals prior to the removal of the troposphere, thus illustrating the signature of an unmodeled troposphere. Figure 9 displays the elevation profile over the pass and the troposphere model that was fit from the data of Fig. 8 and then removed from the residuals, resulting in the plots displayed in Figs. 4–7. Figure 10 displays the TSAC ionosphere correction at 2.3 GHz for this pass.

Table 3. Ulysses media calibration test results.

| Pass, yr-day	DSS	ION	TRP	Zenith path delay, m	Linear slope, 10^{-7} Hz/s	$\sigma_y(1)$, 10^{-14}	$\sigma_y(10)$, 10^{-14}	$\sigma_y(100)$, 10^{-14}	$\sigma_y(1000)$, 10^{-14}
91-004 S	14	T	F	1.50 ± 0.06	-0.001 ± 0.71	1080	116	15.4	4.8
91-004 S	14	D	F	1.90 ± 0.08	0.08 ± 1.71	2624	276	32.5	2.4
91-004 S	14	N	F	0.44 ± 0.06	0.09 ± 0.71	1081	116	15.4	6.2
91-004 S	14	T	M	2.1	1.35 ± 0.71	1081	116	15.4	6.7
91-004 X	14	T	F	1.69 ± 0.03	0.29 ± 1.65	621	66	9.3	1.9
91-004 X	14	D	F	1.40 ± 0.04	0.65 ± 1.83	756	80	12.8	3.7
91-004 X	14	N	F	1.05 ± 0.04	0.42 ± 1.65	621	66	9.3	2.8
91-004 X	14	T	M	2.1	3.51 ± 1.65	621	66	9.3	3.6
91-004 SX	14	T	N	—	0.66 ± 0.67	1107	116	13.3	3.3
91-004 SX	14	N	N	—	1.51 ± 0.67	1107	116	13.4	5.2
92-064 S	14	T	F	1.54 ± 0.05	0.19 ± 0.12	335	46	16.7	6.7
92-064 S	14	D	F	1.65 ± 0.04	-0.004 ± 0.12	384	45	16.4	7.4
92-064 S	14	N	F	1.17 ± 0.04	0.13 ± 0.12	335	46	16.7	5.9
92-064 S	14	T	M	2.1	1.26 ± 0.12	335	46	16.7	6.6
92-064 X	14	T	F	1.43 ± 0.03	0.12 ± 0.25	147	30	13.6	5.6
92-064 X	14	D	F	1.46 ± 0.04	0.15 ± 0.27	187	31	13.8	6.1
92-064 X	14	N	F	1.38 ± 0.04	0.23 ± 0.25	147	30	13.6	5.7
92-064 X	14	T	M	2.1	4.63 ± 0.24	147	30	13.6	6.2
92-064 SX	14	T	N	—	0.15 ± 0.09	303	32	9.4	4.1
92-064 SX	14	N	N	—	0.49 ± 0.09	303	32	9.4	4.1
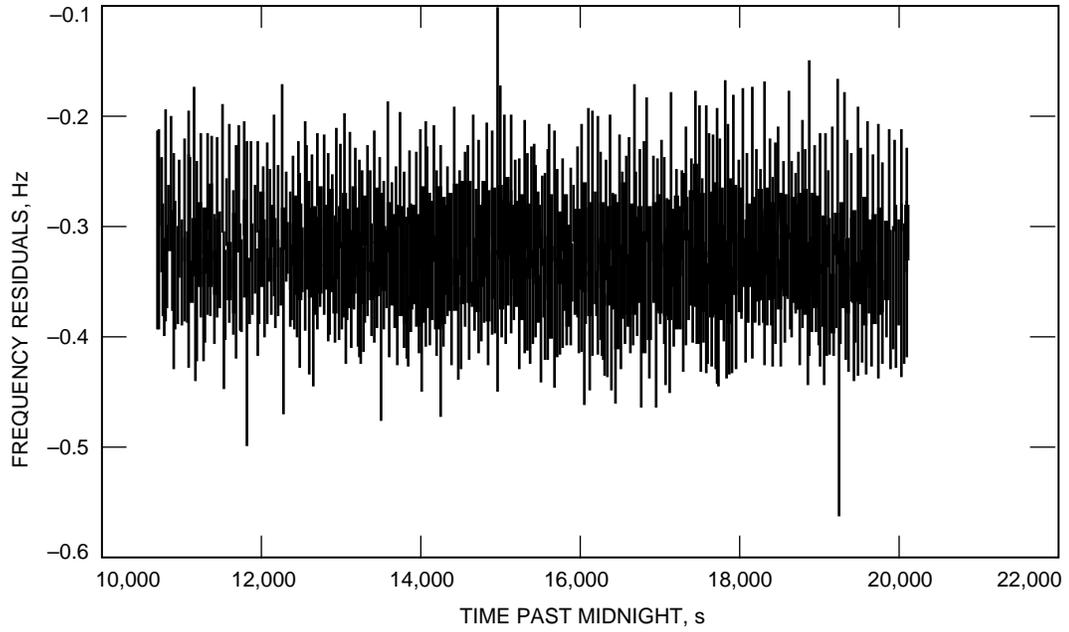
Fig. 4. An example of 8.4-GHz frequency residuals from a Ulysses pass conducted
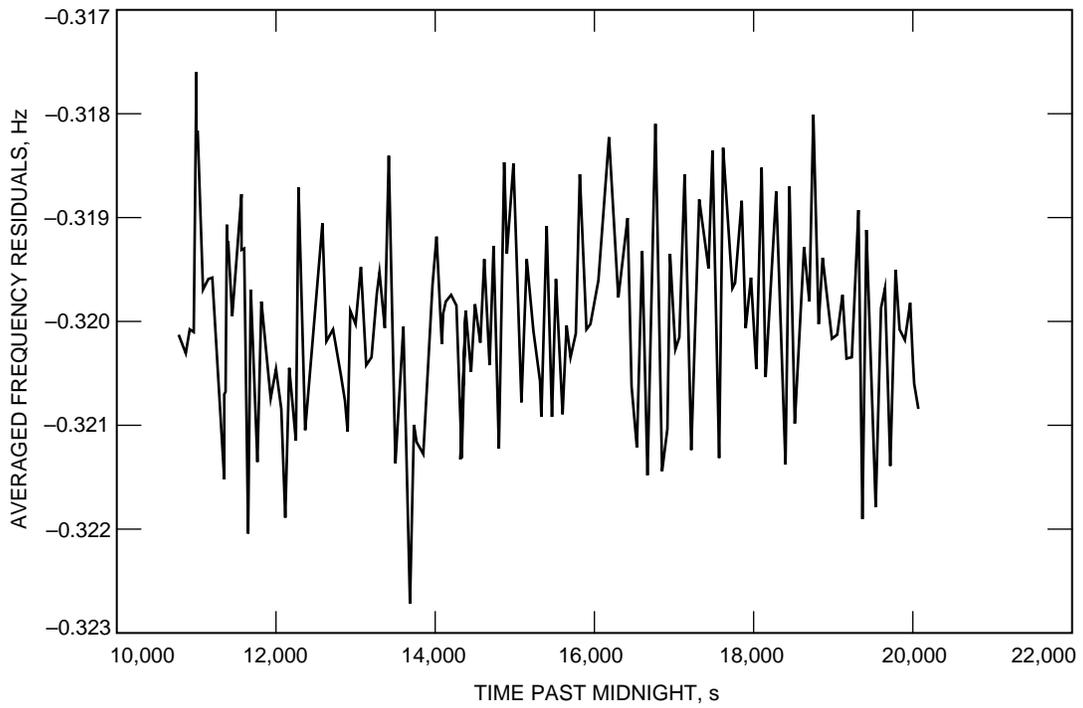at DSS 14 on January 4, 1991.

Fig. 5. An example of 8.4-GHz frequency residuals from Fig. 4 averaged every 60 s from
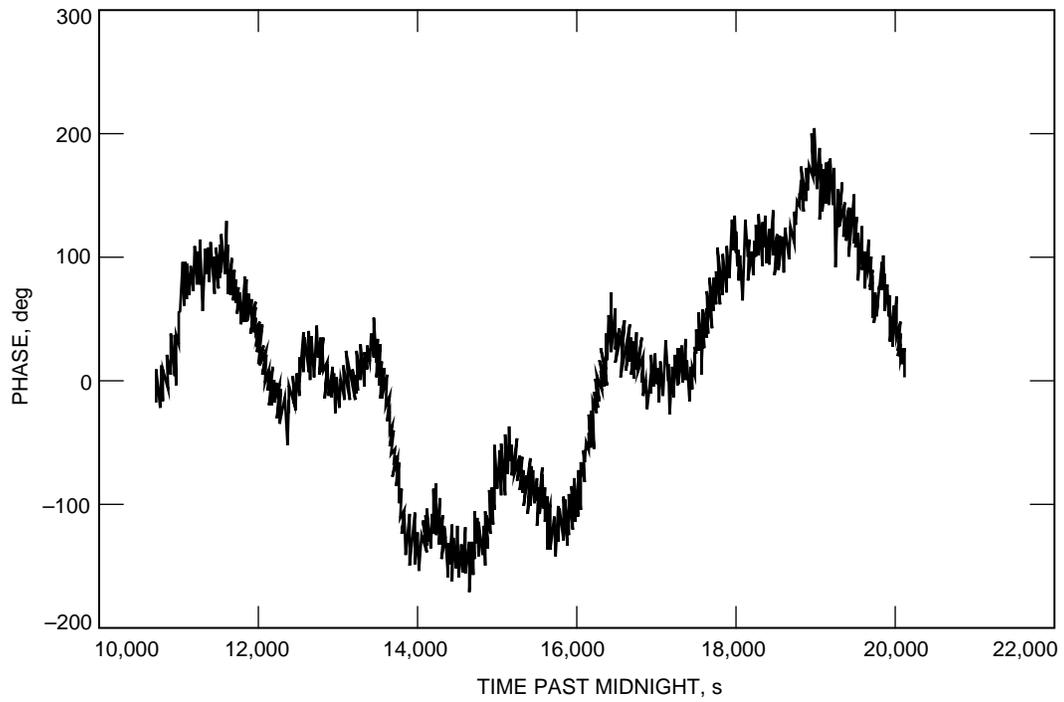a Ulysses pass conducted at DSS 14 on January 4, 1991.

Fig. 6. An example of phase reconstructed from the frequency residuals of Fig. 4.
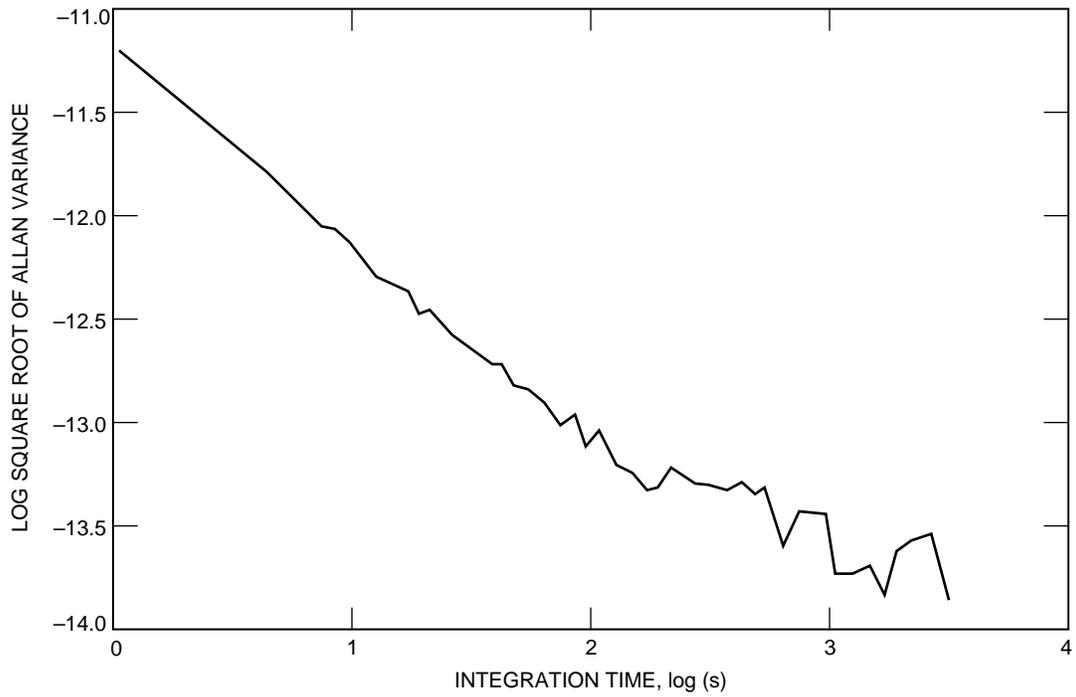

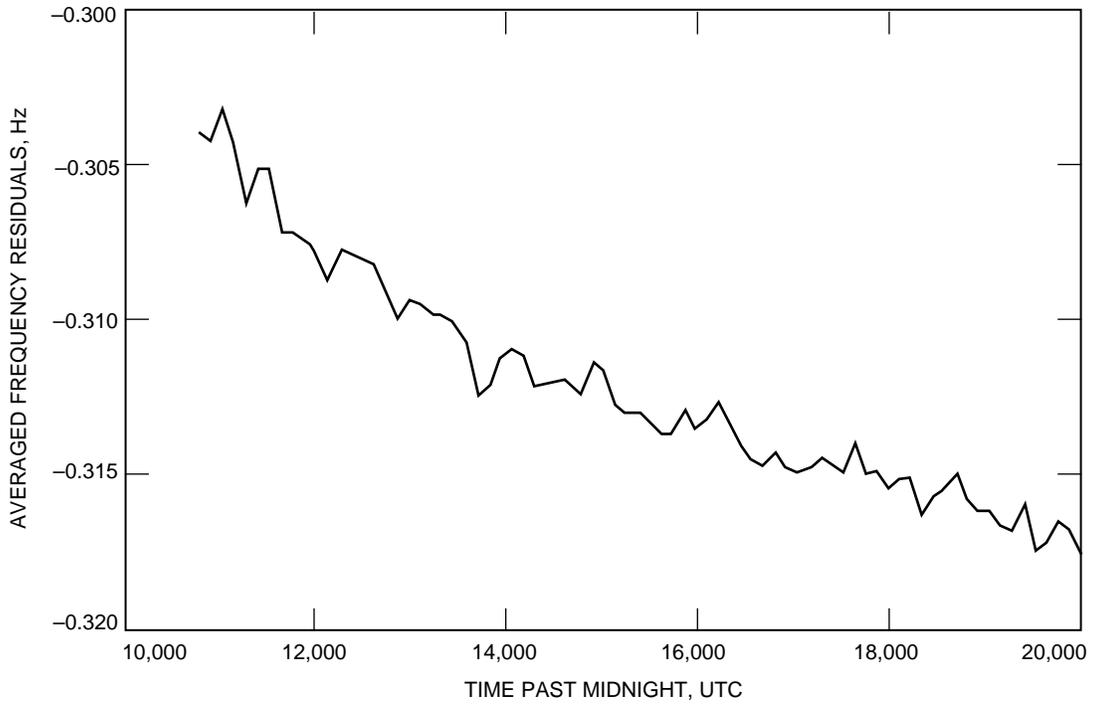**Fig. 7. An example of Allan deviations of the frequency residuals of Fig. 4.**

Fig. 8. An example of averaged frequency residuals from a Ulysses pass conducted at DSS 14 on January 4, 1991, without calibrating troposphere.
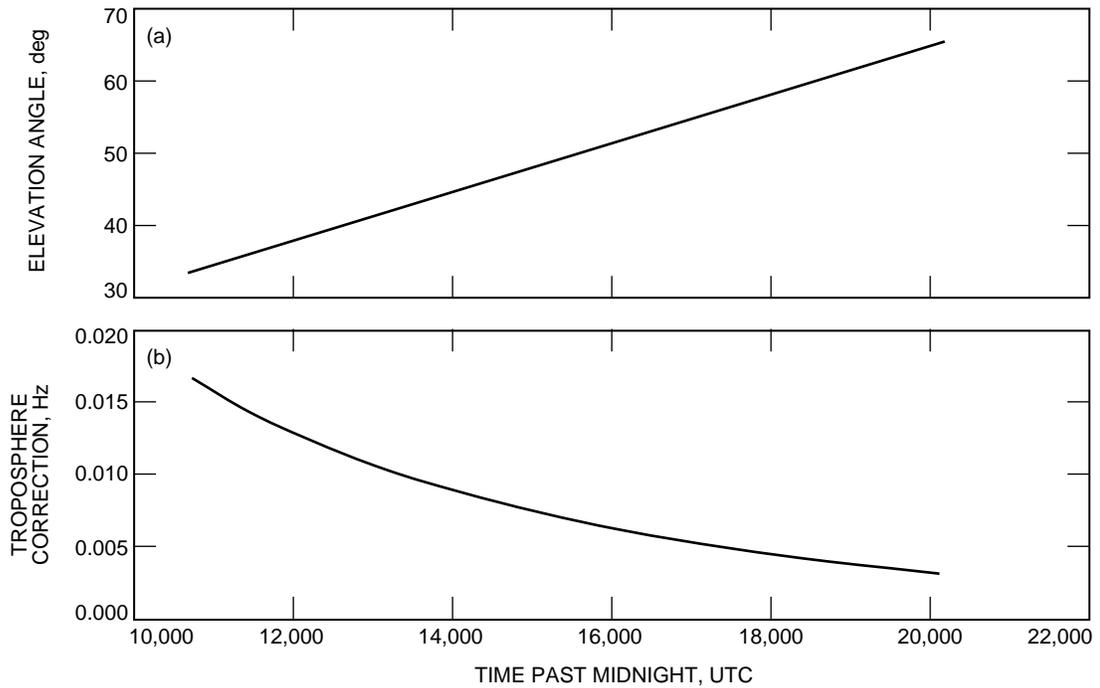
Fig. 9. The (a) elevation angle profile and (b) troposphere correction fit from the frequency residuals of Fig. 8. This signature was then removed from the data, resulting in the calibration illustrated in Figs. 4 through 7.
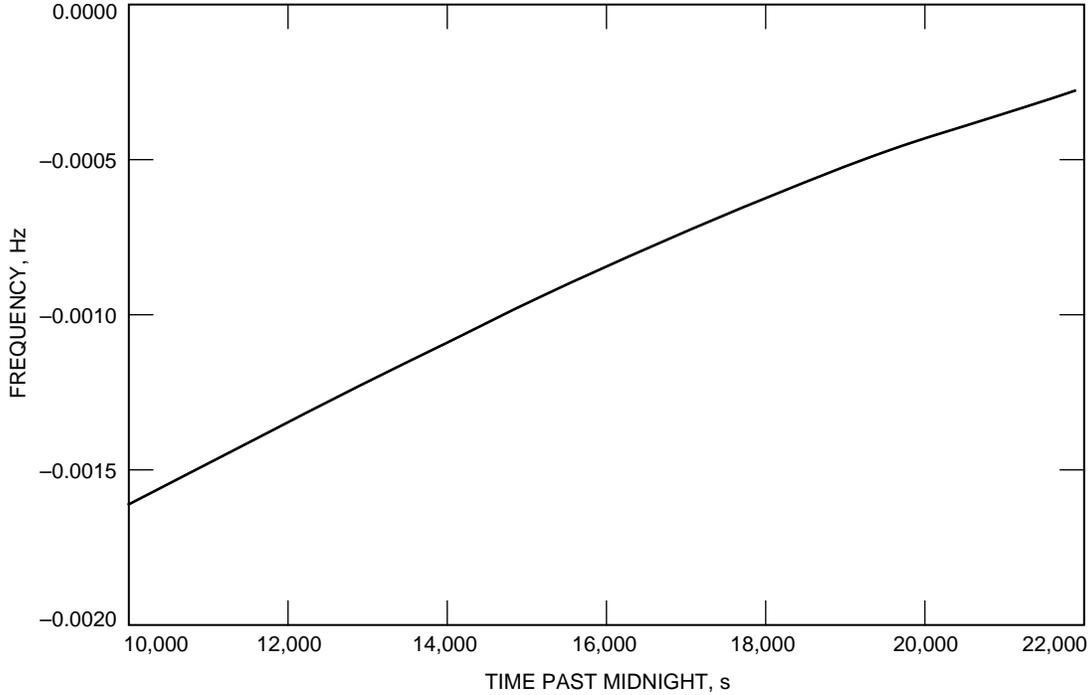
Fig. 10. Ionosphere frequency correction at 2.3 GHz, derived from a TSAC polynomial for the DSS-14 Ulysses pass of January 4, 1991.

The fitted zenith path delays for case (T,F) appear reasonable but are somewhat low compared to the expected 2.1-m values. Unmodeled trends, which blend with the signature of the troposphere, are assumed to exist in the data and thus influence the fit.

The linear slope from a straight line least-squares fit of the postcalibrated residuals tends to be of insignificant or of marginal magnitude when a troposphere fit is performed. When a model troposphere is removed, the fitted linear slopes of the residuals are significant. This suggests that significant unknown trends may be present in the data set that are absorbed by the troposphere fit or that the troposphere model using the default zenith path delay is not sufficient.

The Allan deviations at 1, 10 and 100 s do not change significantly between the different runs for a given band, except for the dual-frequency charged-particle calibrated runs (D in the ION column), where significant system noise at these time intervals is introduced into the data. At 1000 s, dual-frequency charged-particle calibration (D,F) results in the lowest Allan deviations at 2.3 GHz for the 91-004 pass and no significant changes at 2.3 GHz for pass 92-064. At 8.4 GHz, the TSAC calibrated run for pass 91-004 produced the lowest Allan deviation, 1.9×10^{-14}. For the 92-064 DSS-14 pass, no significant improvement was noted in the 8.4-GHz 1000-s Allan deviation between the different runs. The 91-004 Allan deviations agree with independently measured values [4].

For the $f^s - 3f^x/11$ data type (SX), the following runs were performed: (1) TSAC correction [Eq. (25)](T) and no troposphere (N) and (2) no ionosphere calibration (N) and no troposphere calibration (N). Since the difference frequency eliminates all nondispersive effects, troposphere calibration is not performed. For 91-004 SX and 92-064 SX, the slopes of the calibrated runs were of insignificant or marginal magnitudes, suggesting the effectiveness of using TSAC polynomials to remove long period trends from the SX data type and illustrating the dominance of the time variability of the ionosphere over that of the solar plasma during these observations near solar opposition. The Allan deviations do not change significantly between runs for the SX data type, except that the 1000-s value for pass 91-004 SX shows an improvement from 5.2×10^{-14} to 3.3×10^{-14} when applying the TSAC calibration.

Figure 11 displays the averaged residuals for this pass without applying TSAC (N,N). Here, all nondispersive effects should cancel out, and the resulting signature is presumably due to dispersive sources. The corresponding TSAC S-X frequency calibration for this pass is shown in Fig. 12. The averaged residuals after applying the TSAC calibration (T,N) are shown in Fig. 13. The resulting signature is considerably flatter than that of the non-TSAC calibration run (N,N) of Fig. 11, but a long period trend of order 0.5-mHz over this pass is apparent upon closer inspection. This is consistent with the observation of Bertotti et al. [4] that the error of the TSAC calibration is not negligible and can be as large as 0.5 mHz. The long period trends on the order of 0.5 mHz that remain in the data after applying media calibrations are consistent with known uncertainties in the calibration schemes. The zenith path delays for the TSAC ionosphere can be in error by as much as 75 cm for day passes and 15 cm for night passes. The troposphere can be in error by 5 cm.[9] An overall 15-cm zenith path delay error (for these nighttime solar opposition passes) can map into variations at the 1-mHz level over a pass, consistent with what is observed in these data.

For Ulysses at 8.4 GHz, trajectory errors of 0.012 mm/s in velocity at 1000 s translate to Allan deviations at about 4×10^{-14}, which is comparable with the observed values. These are also comparable with expected noise due to media. After removal of the ionosphere and troposphere calibration models, significant random fluctuations in the data remain. These fluctuations have different characteristics with different frequencies, solar elongations, local weather conditions, and local ionospheric variability. These are usually masked by system noise at the lower time intervals, whose magnitudes depend upon received signal levels and received noise power of a given spacecraft. Expected levels of these fluctuations at 1000 s for Ulysses at 8.4 GHz are about 3×10^{-14} for the troposphere, an upper bound of 3×10^{-14} for plasma noise, and 2.5×10^{-14} for the system noise of the closed-loop receiver [4].

Figure 14 displays the 8.4-GHz Allan deviation curves for a set of different calibration schemes for the 91-004 DSS-14 pass. For the case of two-way data over a sufficient elevation angle arc, the best estimate of system stability is obtained by applying a TSAC ionosphere correction and by fitting and removing a troposphere model.

IV. Conclusion

A description of the STBLTY program set has been presented with details on model implementation and residual analysis. Examples of the use of this program set on Galileo and Ulysses data were also presented. The frequency of a spacecraft signal received on the ground is the observable data type. All known effects are removed from this observable to produce residuals that can be inspected to evaluate performance. Among the errors in the residuals are those due to white noise, media, and trajectory. For a sufficiently high SNR, random media effects appear to be the limiting error source at the 1000-s time scale for both Galileo and Ulysses coherent data sets.

Future upgrades to STBLTY will focus on modeling the gravity fields of planets in order to remove these effects from the data during flybys or orbital operations. The first use for this capability will involve the Galileo Jupiter orbital operations when Galileo is expected to tour the Jovian system starting in late 1995. Other future upgrades include modifying the code to process 32.0-GHz downlink data such as that expected for the Cassini radio science experiments, to process coherent downlink data that involve 8.4- or 32.0-GHz (Ka-band) uplink signals, converting the code to manipulate vectors in the J2000 system, and incorporating a planetary atmospheric model for occultation data analysis. The program set was recently modified to process three-way data (implemented in a developmental version).

---

[9] T. McElrath, personal communication, Navigation Systems Section, Jet Propulsion Laboratory, Pasadena, California, 1994.
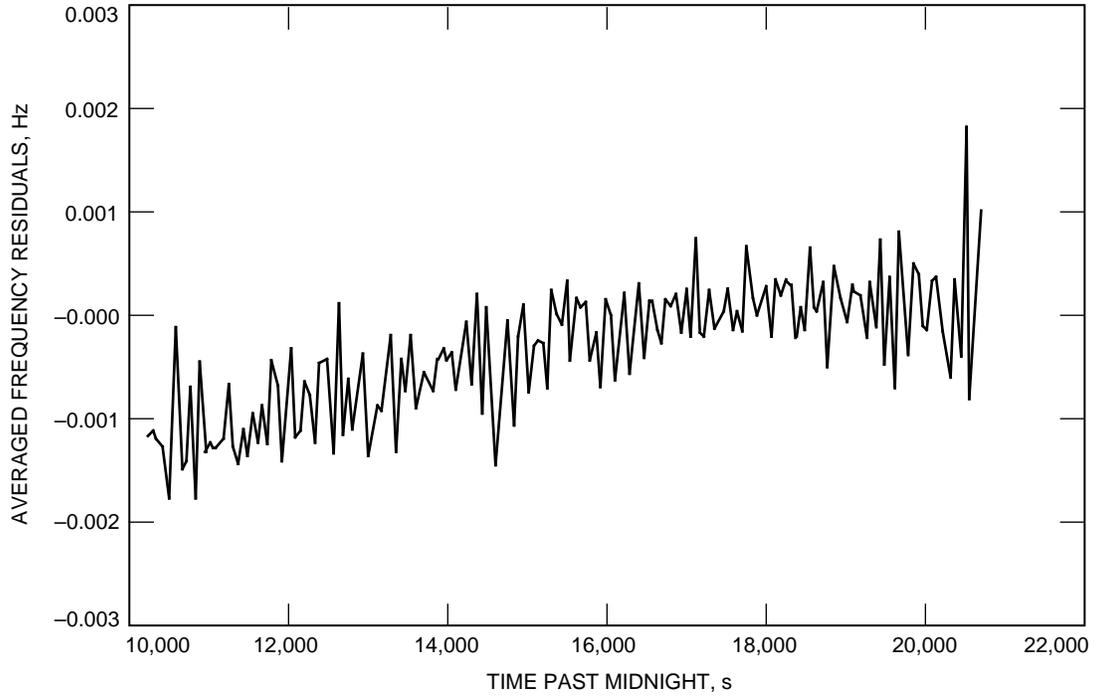
Fig. 11. Averaged differenced frequency residuals (dual-band) for the DSS-14 Ulysses pass of January 4, 1991.
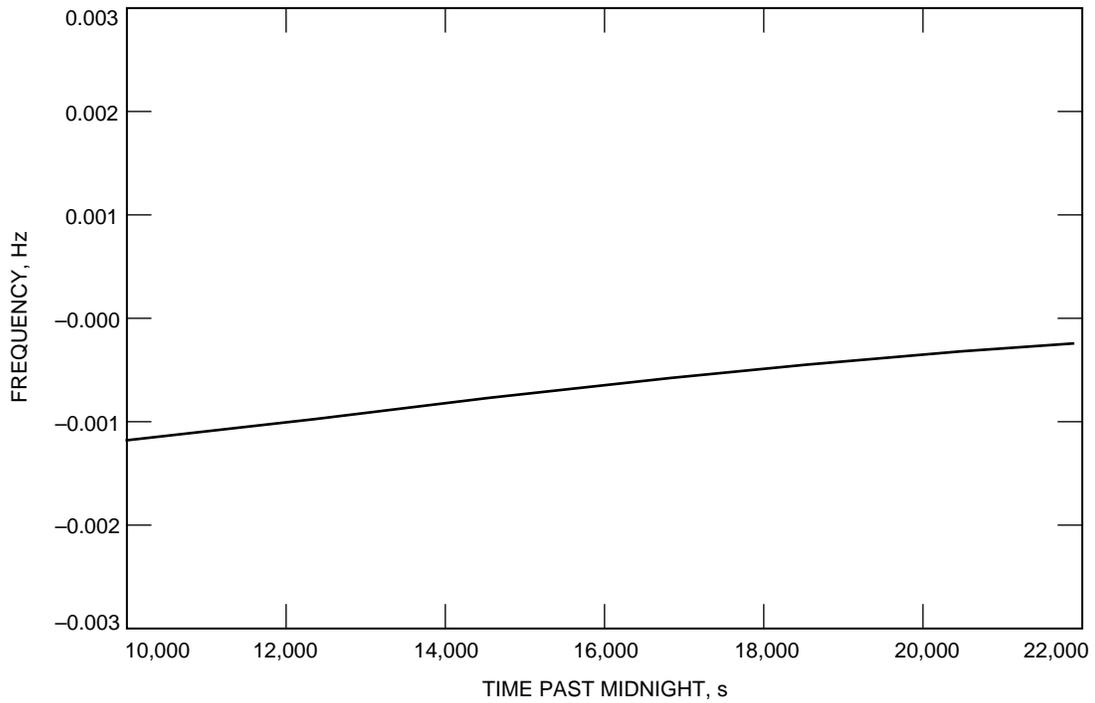

Fig. 12. Ionosphere frequency correction for dual-band derived from a TSAC polynomial for the DSS-14 Ulysses pass of January 4, 1991.
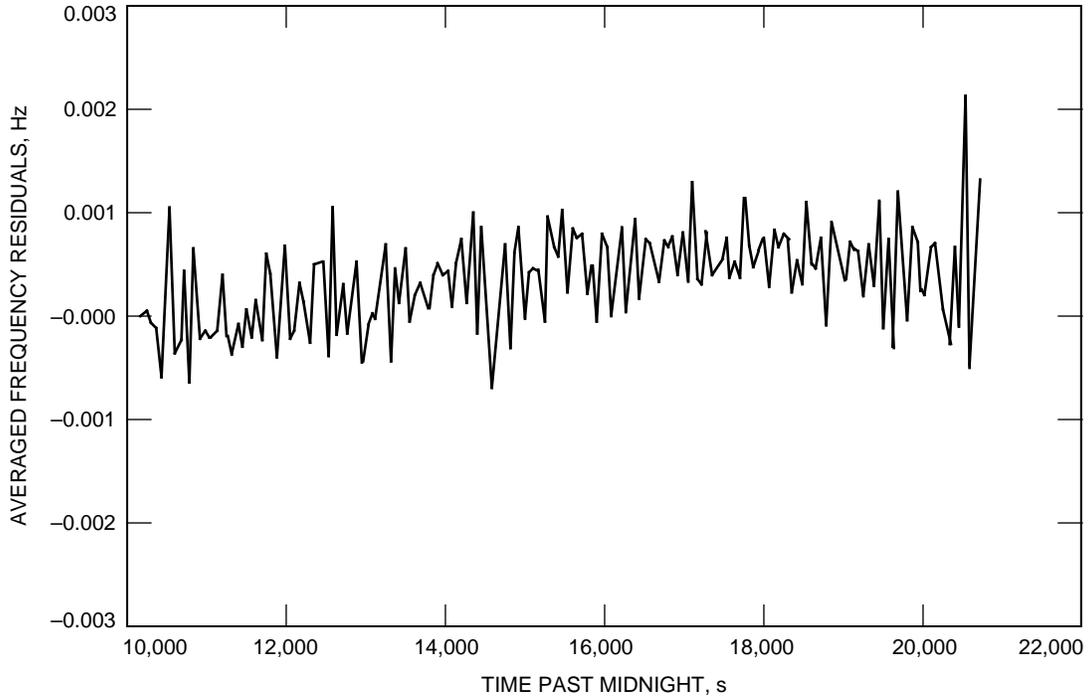
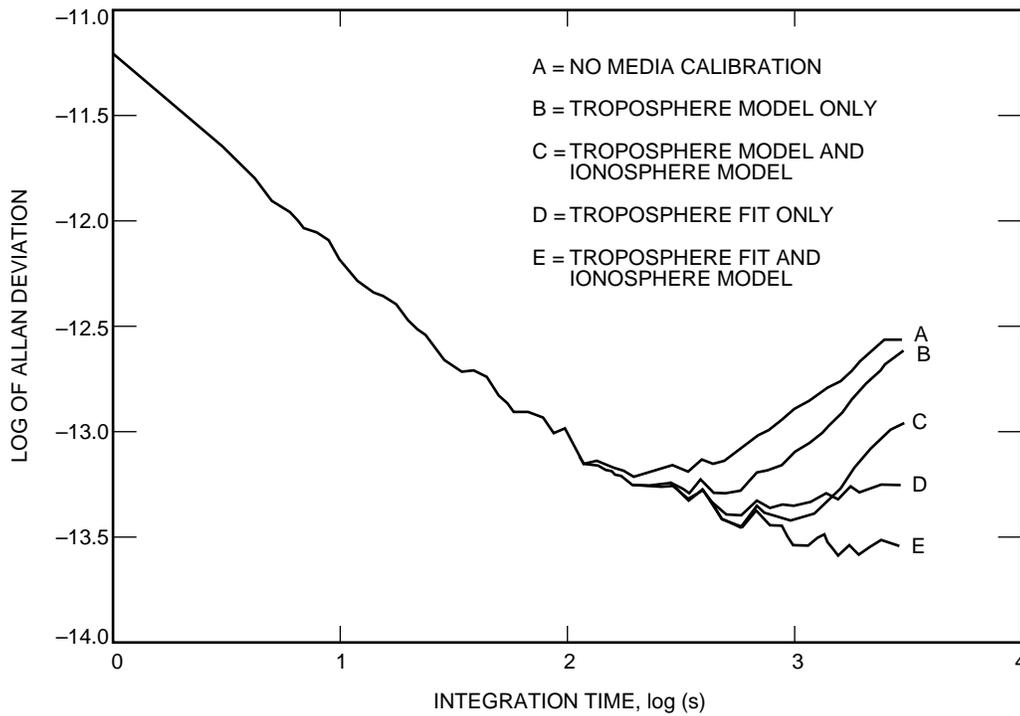**Fig. 13. Averaged differenced frequency residuals (dual-band) of Fig. 11 after removing the TSAC correction of Fig. 12.**

A = NO MEDIA CALIBRATION

B = TROPOSPHERE MODEL ONLY

C = TROPOSPHERE MODEL AND IONOSPHERE MODEL

D = TROPOSPHERE FIT ONLY

E = TROPOSPHERE FIT AND IONOSPHERE MODEL

Fig. 14. Allan deviation curves for a set of different calibration schemes for the DSS-14 Ulysses pass of January 4, 1991.

Acknowledgments

References

[1] T. P. Krisher, D. D. Morabito, and J. D. Anderson, "The Galileo Solar Redshift Experiment," *Physical Review Letters*, vol. 70, pp. 2213–2216, April 12, 1993.

[2] J. D. Anderson, J. W. Armstrong, J. K. Campbell, F. B. Estabrook, T. P. Krisher, and E. L. Lau, "Gravitation and Celestial Mechanics Investigations With Galileo," *Space Science Review*, vol. 60, pp. 591–610, 1992.

[3] D. D. Morabito, T. P. Krisher, and S. W. Asmar, "The Flight Performance of the Galileo Orbiter USO," *Proceedings of the IEEE Frequency Control Symposium*, IEEE Catalog No. 93CH3244-1, Salt Lake City, Utah, pp. 788–805, June 2–4, 1993.

[4] B. Bertotti, R. Ambrosini, S. W. Asmar, J. P. Brenkle, G. Comoretto, G. Giampieri, L. Iess, A. Messeri, R. Vecchio, and H. D. Wahlquist, *Ulysses Gravitational Wave Experiment Report on the First Opposition*, IFI-91-25, Istituto di Fisica dello Spazio Interplanetario, Frascati, Italy, December 1991.

[5] H. T. Howard, V. R. Eshleman, D. P. Hinson, A. J. Kliore, G. F. Lindal, R. Woo, M. K. Bird, H. Volland, P. Edenhofer, M. Pätzold, and H. Porche, "Galileo Radio Science Investigation," *Space Science Review*, vol. 60, pp. 565–590, 1992.

[6] A. C. Densmore, "A Digitally Implemented Phase-Locked Loop Detection Scheme for Analysis of the Phase and Power Stability of a Calibration Tone," *The Telecommunications and Data Acquisition Progress Report 42-93, January–March 1988*, Jet Propulsion Laboratory, Pasadena, California, pp. 207–213, May 15, 1988.

[7] T. M. Nguyen, S. M. Hinedi, H.-G. Yeh, and C. Kyriacou, "Performance Evaluation of Digital Phase-Locked Loops for Advanced Deep Space Transponders," *The Telecommunications and Data Acquisition Progress Report 42-117, January–March 1994*, Jet Propulsion Laboratory, Pasadena, California, pp. 175–193, May 15, 1994.

[8] R. M. Jaffee, and E. Rechtin, "Design and Performance of Phase Locked Circuit Capable of Near Optimum Performance Over a Wide Range of Input Signal and Noise Levels," *IRE Transactions on Information Theory*, vol. IT-1, pp. 66–76, March 1955.

[9] V. M. Pollmeier and P. H. Kallemeyn, "Galileo Orbit Determination From Launch Through the First Earth Flyby," *Proceedings of the 47th Annual Meeting of the Institute of Navigation*, Williamsburg, Pennsylvania, pp. 9–16, June 10–12, 1991.

[10] T. McElrath, B. Tucker, P. Menon, E. Higa, and K. Criddle, "Ulysses Navigation at Jupiter Encounter," *AIAA/AAS Astrodynamics Conference Proceedings*, AIAA 92-4524, pp. 1–9, August 10–12, 1992.

[11] C. Yoder, J. G. Williams, and M. Parke, "Tidal Variations of Earth Rotation," *Journal of Geophysical Research*, vol. 86, p. 881–891, 1981.

[12] P. K. Seidelmann, "1980 IAU Theory of Nutation: The Final Report of the IAU Working Group on Nutation," *Celestial Mechanics*, vol. 27, p. 79–106, 1982.

[13] D. D. McCarthy and B. J. Luzan, "Observations of Luni-Solar and Free Core Nutation," *Astronomical Journal*, vol. 102, no. 5, pp. 1889–1895, November 1991.

[14] J. L. Davis, T. A. Herring, I. I. Shapiro, A. E. E. Rogers, and G. Elgered, "Geodesy by Radio Interferometry: Effects of Atmospheric Modeling Error on Estimated Baseline Length," *Radio Science*, vol. 20, pp. 1593–1607, 1985.

[15] G. Lanyi, "Tropospheric Delay Effect in Radio Interferometry," *The Telecommunications and Data Acquisition Progress Report 42-78, April–June 1984*, Jet Propulsion Laboratory, Pasadena, California, pp. 152–159, August 15, 1984.

[16] J. W. Armstrong, R. Woo, and F. B. Estabrook, "Interplanetary Phase Scintillation and the Search for Very Low Frequency Gravitational Radiation," *Astrophysical Journal*, vol. 230, pp. 570–574, June 1, 1979.

Appendix

Formulation of Precession and Nutation Matrices

The following definitions for system rotation matrices and their derivatives apply when defining the precession and nutation rotation matrices and their derivatives:

$$(\theta)_x = \begin{bmatrix} 1 & 0 & 0 \\ 0 & \cos\theta & \sin\theta \\ 0 & -\sin\theta & \cos\theta \end{bmatrix} \quad \frac{d}{dt}(\theta)_x = \begin{bmatrix} 0 & 0 & 0 \\ 0 & -\sin\theta & \cos\theta \\ 0 & -\cos\theta & -\sin\theta \end{bmatrix} \dot\theta = \left(\frac{\pi}{2} - \theta\right)_x \dot\theta$$

$$(\theta)_z = \begin{bmatrix} \cos\theta & \sin\theta & 0 \\ -\sin\theta & \cos\theta & 0 \\ 0 & 0 & 1 \end{bmatrix} \quad \frac{d}{dt}(\theta)_z = \begin{bmatrix} -\sin\theta & \cos\theta & 0 \\ -\cos\theta & -\sin\theta & 0 \\ 0 & 0 & 0 \end{bmatrix} \dot\theta = \left(\frac{\pi}{2} - \theta\right)_z \dot\theta$$

I. Precession Rotation Formulation

The precession matrix, $\mathbf{P}$, is the product of the following three system rotations using the definitions given above:

$$\mathbf{P} = \left(\frac{\pi}{2} - \alpha_{1950}\right)_z \left(\frac{\pi}{2} - \delta_{1950}\right)_x (-\Delta_{1950})_z$$

where the precession rotation angles in terms of Julian centuries since 1950, T, are given by

$$\Delta_{1950} = [89.9999986565 - 0.64027801T - (3.042075 \times 10^{-4})T^2 - (5.0837 \times 10^{-6})T^3]\frac{\pi}{180}$$

$$\delta_{1950} = [89.9999988317 - 0.5567500297T + (1.185607 \times 10^{-4})T^2 + (1.16119 \times 10^{-5})T^3]\frac{\pi}{180}$$

$$\alpha_{1950} = [(-1.3435 \times 10^{-6}) - 0.6402780091T - (8.39481 \times 10^{-5})T^2 - (0.50003 \times 10^{-5})T^3]\frac{\pi}{180}$$

The derivative of the precession matrix is as follows:

$$\dot{\mathbf{P}} = (\pi - \alpha_{1950})_z \left(\frac{\pi}{2} - \delta_{1950}\right)_x (-\Delta_{1950})_z \left[\frac{-d}{dt}\alpha_{1950}\right]$$

$$+ \left(\frac{\pi}{2} - \alpha_{1950}\right)_z (\pi - \delta_{1950})_x (-\Delta_{1950})_z \left[\frac{-d}{dt}\delta_{1950}\right]$$

$$+ \left(\frac{\pi}{2} - \alpha_{1950}\right)_z \left(\frac{\pi}{2} - \delta_{1950}\right)_x \left(\frac{\pi}{2} - \Delta_{1950}\right)_z \left[\frac{-d}{dt}\Delta_{1950}\right]$$

where

$$\frac{d}{dt}\Delta_{1950} = [-0.64027801 - (2 \times 3.042075) \times 10^{-4}T - (3 \times 5.0837) \times 10^{-6}T^2]\frac{\pi}{180}$$

$$\frac{d}{dt}\delta_{1950} = [-0.5567500297 + (2 \times 1.185607) \times 10^{-4}T + (3 \times 1.16119) \times 10^{-5}T^2]\frac{\pi}{180}$$

$$\frac{d}{dt}\alpha_{1950} = [-0.6402780091 - (2 \times 8.39481) \times 10^{-5}T - (3 \times 0.50003) \times 10^{-5}T^2]\frac{\pi}{180}$$

II. Nutation Rotation Formulation

The nutation rotation matrix is the product of the following three rotations using the matrix rotation definitions given above:

$$\mathbf{N} = (-\epsilon_m)_x (\Delta\Psi)_z (\epsilon_m + \Delta\epsilon)_x$$

where the nutation angles are the IAU 1980 model values defined in the text. The derivative of the nutation rotation matrix is thus given as

$$\dot{\mathbf{N}} = -\dot{\epsilon}\left(\epsilon_m + \frac{\pi}{2}\right)_x (\Delta\Psi)_z (\epsilon_m + \Delta\epsilon)_x + \Delta\dot{\Psi}(-\epsilon_m)_x \left(-\Delta\Psi + \frac{\pi}{2}\right)_z$$

$$\times (\epsilon_m + \Delta\epsilon)_x + \dot{\epsilon}(-\epsilon_m)_x (\Delta\Psi)_z \left(-\epsilon_m - \Delta\epsilon + \frac{\pi}{2}\right)_x$$